

FINAL  
1N-38-CR  
OCT.  
43778

WASHINGTON UNIVERSITY  
DEPARTMENT OF PHYSICS  
LABORATORY FOR ULTRASONICS  
St. Louis, Missouri 63130

**"Application of Linear Array Imaging Techniques to the Real-Time Inspection of  
Airframe Structures and Substructures"**

Final Progress Report: April 15, 1996

NASA Grant Number: NSG-1601

Principal Investigator:

Dr. James G. Miller  
Professor of Physics

The NASA Technical Officer for this grant is:

Dr. Patrick H. Johnston  
NASA Langley Research Center  
Hampton, Virginia

# **Application of Linear Array Imaging Techniques to the Real-Time Inspection of Airframe Structures and Substructures**

<b>I.</b>	<b>Introduction .....</b>	<b>1</b>
<b>II.</b>	<b>Detection of Disbonded Regions (flat-bottom holes) in Bonded Aluminum Plates....</b>	<b>2</b>
<b>III.</b>	<b>Detection of Disbonded Regions (adhesive tape) in Bonded Aluminum Plates.....</b>	<b>4</b>
<b>IV.</b>	<b>Comparison of Disbond Images .....</b>	<b>18</b>
<b>V.</b>	<b>Comparison of Linear Array Detection of Disbond Regions in Bonded Aluminum Plates With Contact Measurements (Analytic Signal) .....</b>	<b>28</b>
<b>VI.</b>	<b>Linear Array Inspection of Typical "Flaws" Encountered in Aircraft Structures ...</b>	<b>42</b>

## **I. Introduction**

Current concern for ensuring the air-worthiness of the aging commercial air fleet has prompted the establishment of broad-agency programs to develop NDT technologies that address specific aging-aircraft issues.<sup>1,2</sup> One of the crucial technological needs that has been identified is the development of rapid, quantitative systems for depot-level inspection of bonded aluminum lap joints on aircraft.<sup>1-3</sup> Research results for characterization of disbond and corrosion based on normal-incidence pulse-echo measurement geometries are showing promise, but are limited by the single-site nature of the measurement which requires manual or mechanical scanning to inspect an area.<sup>4-7</sup> One approach to developing efficient systems may be to transfer specific aspects of current medical imaging technology to the NDT arena. Ultrasonic medical imaging systems offer many desirable attributes for large scale inspection. They are portable, provide real-time imaging, and have integrated video tape recorder and printer capabilities available for documentation and post-inspection review. Furthermore, these systems are available at a relatively low cost (approximately \$50,000 to \$200,000) and can be optimized for use with metals with straight-forward modifications. As an example, ultrasonic phased-array and linear array imaging technology, which was first developed for use in the medical industry, has been successfully implemented for some NDT applications by other investigators.<sup>8-10</sup>

In this Progress Report we summarize the results from our investigation into the feasibility of implementing medical linear array imaging technology as a viable ultrasonic-based nondestructive evaluation method to inspect and characterize bonded aluminum lap joints.

## **II. Detection of Disbonded Regions (flat-bottom holes) in Bonded Aluminum Plates**

A commercially available clinical medical linear array imaging system was used to image disbonds and simulated "corrosion" in bonded aluminum plates. Four bonded aluminum plate test specimens were investigated with a 7.5 MHz linear array and the resultant images recorded in real-time on video tape. Two of the specimens were manufactured in our Laboratory and consisted of 0.050-inch aluminum plates bonded together with type PR-1422 sealant obtained from Trans-World Airlines. In each of these two specimens one of the bonded aluminum plates had four regions of simulated corrosion consisting of 0.025-inch deep flat-bottom holes with diameters of 1.000, 0.500, 0.250, and 0.125-inches, all backfilled with Styrofoam. These bonded plates also had a region with a plastic strip and no sealant between the plates to represent a disbonded region. The other two specimens consisted of 0.040-inch thick bonded aluminum plates which were constructed at NASA Langley Research Center. These bonded plates had square holes milled into one of the plates prior to assembly which were intended to simulate a corroded and disbonded region .

Preliminary results, comparing the images of the bonded aluminum plate specimens obtained with the linear array with the corresponding ultrasonic rf A-lines obtained using a contact transducer, suggest that linear array imaging can play a useful role in detecting disbonded regions and providing information describing bond interface characteristics. The disbonded regions were easily discernible from the well-bonded regions in the images obtained from either side of each specimen. Images of the specimens show that the disbonded regions appear much different when the images obtained from the "bottom" of the specimen are compared with those obtained from the "top". Our preliminary results show that a relatively "bright" disbond region observed when the specimens are imaged from the "bottom" side and a "dark" disbond region observed when the specimens are imaged from the "top" side agree with the corresponding echo decay patterns obtained with the contact transducer; i.e., a relatively higher attenuation associated with the disbonded region when interrogated from the "top" when compared with the results obtained from the "bottom". Subsequent destructive analysis of the specimens indicated that the "bottom" plate was in direct contact with the adhesive of the masking tape (as expected) but the "top" plate had a thin substance adhered to it. These preliminary results suggest that the images obtained with the linear array may convey information regarding the characteristics of the interface between the aluminum and the disbond.

Many aspects of the images of the well-bonded regions of the specimens obtained with the SONOS 1500 linear array are consistent with the contact transducer data. Modulations of the brightness of the well-bonded region in the images of specific specimens agree with the observed



modulations in the echo decay patterns obtained with the contact transducer. Image patterns of specimens that have aluminum plates of different thicknesses are consistent with the measured rf A-lines of these specimens. The images and corresponding rf A-lines of these specimens show that the well-bonded regions appear different when interrogated from the "bottom" side and compared with the image from the "top" side. This difference between the two sides is evident in the measured echo decay patterns obtained.

These preliminary measurements<sup>11</sup>, showing the linear-array images of the bonded aluminum plate specimens and the corresponding agreement with contact transducer measurements, suggest that linear array technology may provide a viable means to detect disbonded regions in bonded aluminum joints. Furthermore, these images may provide useful information regarding the nature of the disbonded region. It appears that medical linear array imaging technology may offer a useful means to develop a rapid, real-time, and portable method of adhesive bond inspection and characterization.

### **III. Detection of Disbonded Regions (adhesive tape) in Bonded Aluminum Plates**

In this section of the Progress Report we explore the feasibility of implementing medical linear array imaging technology as a viable ultrasonic-based nondestructive evaluation method to inspect and characterize bonded aluminum lap joints. We present images, obtained using an unmodified medical ultrasonic imaging system, of two epoxy-bonded aluminum plate specimens, each with intentionally disbonded regions. These images are compared with corresponding conventional ultrasonic contact transducer measurements in order to assess whether these images can detect disbonded regions and provide information regarding the nature of the disbonded region.

#### ***Background***

The images of the bonded aluminum specimens presented below were obtained using an unmodified, commercially-available Hewlett-Packard SONOS 1500 medical imaging system. Because of the nature of detecting disbonded regions in relatively thin aluminum specimens, the SONOS 1500 imaging system was operated in a mode normally employed to image peripheral blood vessels in a clinical setting. In this peripheral vascular imaging mode, the SONOS 1500 utilizes a linear array of ultrasonic transducer elements as the interrogating probe. A B-scan (cross-sectional) image of the object under interrogation is formed by sequentially transmitting and receiving with groups of transducer elements across the array. Each transmission of an ultrasonic pulse and the subsequent reception of the returned signals by a specific group of transducers represents one ultrasonic A-line in a direction normal to the array. The B-scan image is produced from a series of A-lines across the aperture of the array. Transmit and receive focus is achieved by selecting the appropriate groups of transducer elements and adjusting the relative time of transmit and receive between them. A depth-dependent gain (time-gain compensation or TGC) can be applied to the received ultrasonic signals to reduce the effects of the inherent attenuation of the specimen on the displayed B-scan image.

The B-scan images obtained with the linear array are processed and displayed in a conventional manner. Each received rf A-line signal is mixed to an intermediate frequency, amplified, rectified, and low-pass filtered. The B-scan image, formed from the amplitude envelopes of a series of A-line signals, is logarithmically compressed and displayed as a gray scale image on a dB scale. In general, each B-scan image obtained with a linear array is a cross-sectional representation of the amplitude of the reflected (scattered) ultrasonic signals, in the plane of the array, throughout the depth of the specimen under interrogation. However,

interpretation of the images obtained from layered solids may be expected to be more complex than in tissue because of the presence of strong reverberations and possible mode conversions.

Because the SONOS 1500 system was intended to image specific peripheral blood vessels, it was not possible to change the depth setting of the images to more closely correspond to the thickness dimensions of the bonded aluminum plates. Furthermore, because the thicknesses of the bonded aluminum plate specimens were relatively small and the velocity of sound in aluminum is relatively large (compared to that of tissue), the images obtained with the SONOS 1500 system represent the echo-decay patterns of many round-trip echoes in the plates. Nonetheless, the B-scan images of echo decay patterns in

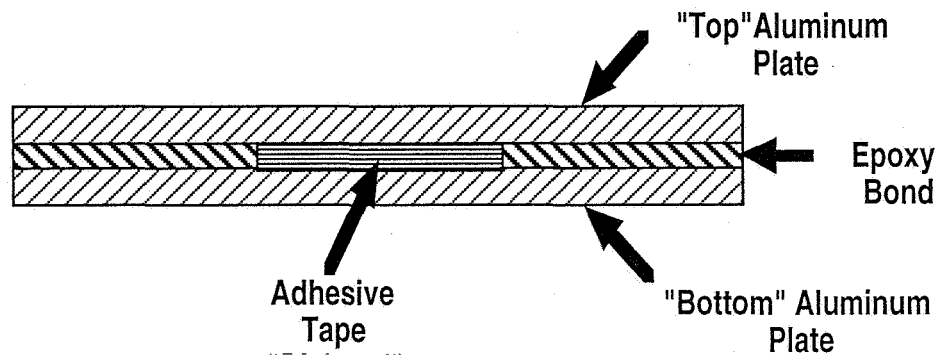


**Figure 1:** Cross-sectional representation of bonded aluminum plate specimen.

bonded aluminum plates appears to represent a viable mode for identifying regions of disbond as will be further discussed below.

### *Specimens*

Both of the bonded aluminum plate specimens interrogated in this investigation were 4.9 cm (1.9 inches) in width by 9.6 cm (3.8 inches) in length. Specimen #1 was constructed using two identical aluminum plates of 0.16 cm (0.063 inch) in thickness; whereas specimen #2 was constructed using one aluminum plate of 0.16 cm (0.063 inch) in thickness and one aluminum plate of 0.23 cm (0.090 inch) in thickness. In each case the specimens were constructed with an area of layered adhesive tape to simulate a disbonded region. These bonded plate specimens were produced by layering adhesive tape in specific areas on one of the plates (referred to as the "bottom" plate) until the layered tape was a specific thickness. For the specimens used in this investigation, layers of masking tape were first applied to the "bottom" plate followed by layers of clear cellophane tape. Epoxy was applied to the "bottom" plate which had the layered

adhesive tape attached and a "top" aluminum plate was applied. After the epoxy had cured the specimens were machined to the final length and width dimensions leaving only one area of simulated disbond transversing the width of the specimen near the center. The width of the disbonded region was 1.27 cm (0.5 inch) for specimen #1 and 2.54 cm (1 inch) for specimen #2. Figure 1 illustrates how these specimens were constructed. Specimen #1 had an epoxy bond thickness of 0.03 cm (0.012 inch) and specimen #2 had an epoxy bond thickness of 0.04 cm (0.016 inch). The measured total thicknesses of the resultant specimens were 0.347 cm (0.136 inches) and 0.424 cm (0.167 inches) for specimens #1 and #2, respectively. In the final configuration the "top" aluminum plate of each specimen was in direct adhesive contact with the epoxy bond everywhere except over the region of the disbond (layered tape). The "bottom" plate

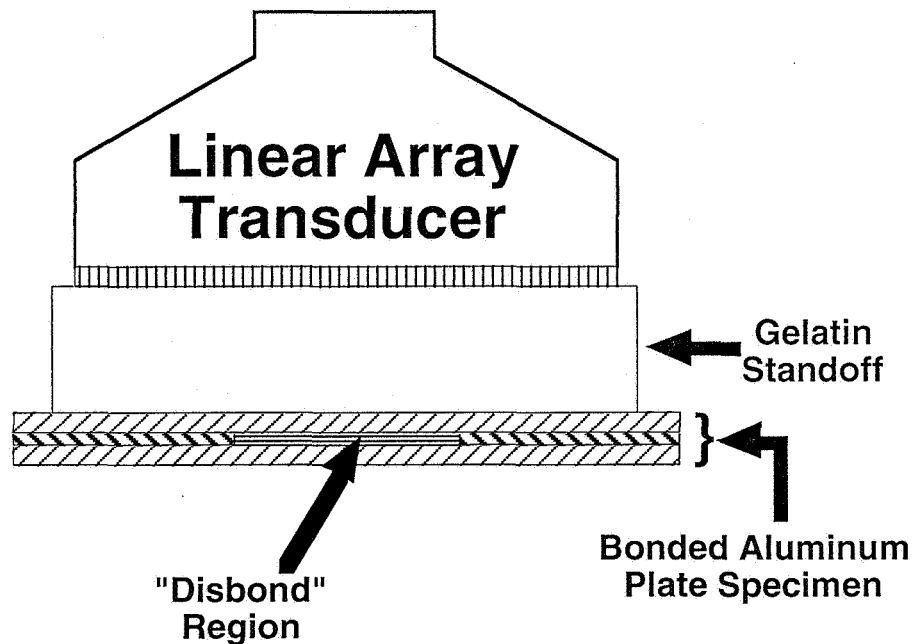


**Figure 2:** Configuration of linear array transducer and gelatin standoff for obtaining images of the disbonded region in the bonded aluminum plate specimens.

was also in direct contact with the epoxy outside the disbond region and in contact with the adhesive side of the masking tape in the region of disbond.

#### *Linear Array Images*

The aluminum plate specimens were imaged with the Hewlett-Packard SONOS 1500 medical imaging system in the peripheral vascular imaging mode described above.

For these measurements a nominal 7.5 MHz center-frequency linear array probe was used with an overall length of 3.9 cm (1.5 inches). Each aluminum plate specimen was imaged with a gelatin stand-off approximately 2.54 cm (1 inch) in thickness between the linear array and specimen as illustrated in Figure 2. The gelatin stand-off was implemented to bring the front surface echo of the aluminum specimens closer to the center of the image. Each specimen was imaged with the axis of the linear array along the long axis (length dimension) of the specimen such that the linear array straddled the disbond region. The SONOS 1500 imaging system was configured such that the transmit power level was kept constant for all measurements and the same depth dependent gain (time-gain compensation) was applied to all depth segments and kept constant between the specimens. The video compression was adjusted to optimize the image contrast and remained constant for each specimen interrogated. The disbanded region and surrounding regions of each specimen were imaged from both sides of the specimen; i.e., each specimen was imaged from the aluminum plate side in contact with the adhesive of the masking tape ("bottom" side) as well as the side with no masking tape adhesive on the plate ("top" side).

Figure 3 illustrates how to interpret the images of the bonded aluminum specimens obtained with the linear array system. The images obtained from both sides of the specimen straddle the disbond region. The disbanded region is represented by the more darkly shaded area in Figure 3. On either side of the disbanded region is the well-bonded region, depicted as the more lightly shaded region in Figure 3. Recall that these images are composed of many reverberations of the ultrasonic signal in the specimen and do not represent a single cross-section.

Figure 4 shows the linear array images over the disbanded region for specimen #1 from both sides. In Figure 4a the region of disbond can be clearly distinguished from the surrounding well-bonded region in the image. This image was obtained from the "bottom" side of the specimen where the masking tape was adhered to the aluminum plate. As described above, the B-scan image represents the returned signals from many round-trip echoes (reverberations) inside the specimen and does not represent a single cross-section through the depth of the specimen. Comparing the disbanded region with the surrounding bonded region in this image it appears that different echo decay patterns can be observed. The echo decay pattern corresponding to the disbanded region appears "brighter" than the surrounding regions and appears to monotonically decrease in brightness as time increases. Furthermore, the individual

# Linear Array Image

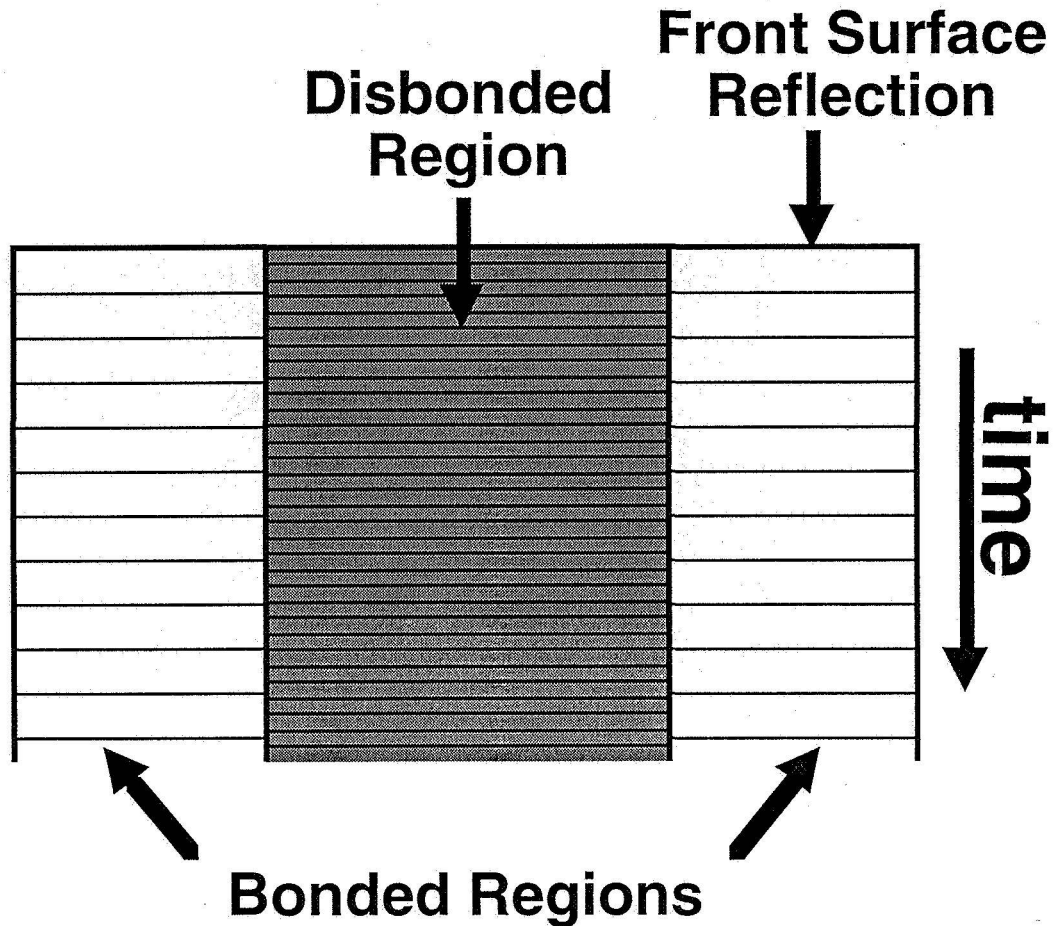


**Figure 3:** Cartoon illustrating how to interpret the linear array images.

echo patterns do not appear as prominent in the disbond region as those observed in the surrounding regions thus giving the disbond region a more "smooth" appearance. The brightness of the echo pattern from the well-bonded region appears to be more modulated and the individual echoes appear more prominently.

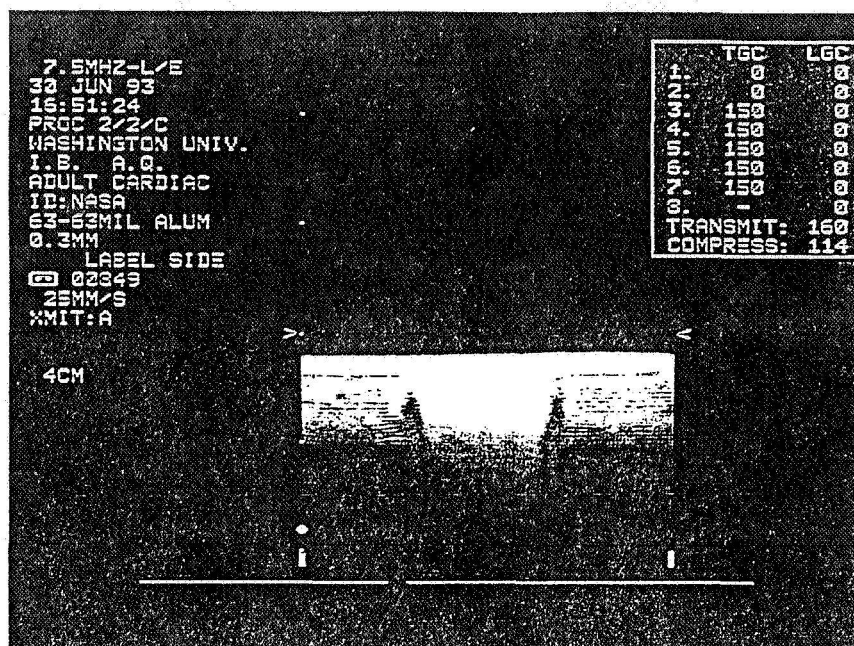
Figure 4b shows the B-scan image of the disbonded region of specimen #1 obtained from the "top" side of the specimen. In this image the region of disbond can again be clearly distinguished from the surrounding well-bonded region although it appears much different than that observed when imaged from the "bottom" side of the specimen (Figure 4a). The image in Figure 4b shows the disbonded region to be much darker than the surrounding well-bonded

regions. This appears to be indicative of a higher attenuation of ultrasound in the disbond region and hence a more rapid rate of echo decay when imaged from the "top" side. Although the disbond region looks very different when Figures 4a and 4b are compared, the well-bonded regions appear to be very similar in the two images. We would expect the images from the well-bonded regions to be very similar when imaged from both sides of the specimen because the thickness of each of the aluminum plates is the same and hence the ultrasound propagates along the same path in both cases.

Figure 5 displays the B-scan images obtained from specimen #2. Figure 5a shows the B-scan image obtained when specimen #2 is interrogated from the "bottom" side of the specimen; the side in which the masking tape was adhered to the "bottom" plate. The image from the "top" side of the specimen is depicted in Figure 5b. The disbond region is again clearly distinguished from the surrounding well-bonded regions in both of these figures. Many of the same features are apparent in these images of specimen #2 as were observed in the images of specimen #1 (Figure 4); e.g., the disbond region appears "brighter" compared to the well-bonded region when specimen #2 is imaged from the "bottom" side (Figure 5a) and much darker than the well-bonded region when imaged from the "top" side (Figure 5b).

There are some interesting differences between the images obtained from specimen #1 and the images obtained from specimen #2 in the well-bonded regions. In contrast to that observed for specimen #1, the echo patterns from the well-bonded regions do not look the same when specimen #2 is interrogated from the "bottom" compared to the images obtained from the "top". The difference in the observed echo pattern corresponding to well-bonded regions may be related to the different thickness of aluminum plate present at the surface of interrogation. The sequence in which a transmitted ultrasonic pulse encounters an aluminum/epoxy interface is different for the two sides of specimen #2. Furthermore, the images of the well-bonded regions of specimen #2 do not appear to have the same modulation pattern of image brightness as observed for specimen #1.

a)



b)

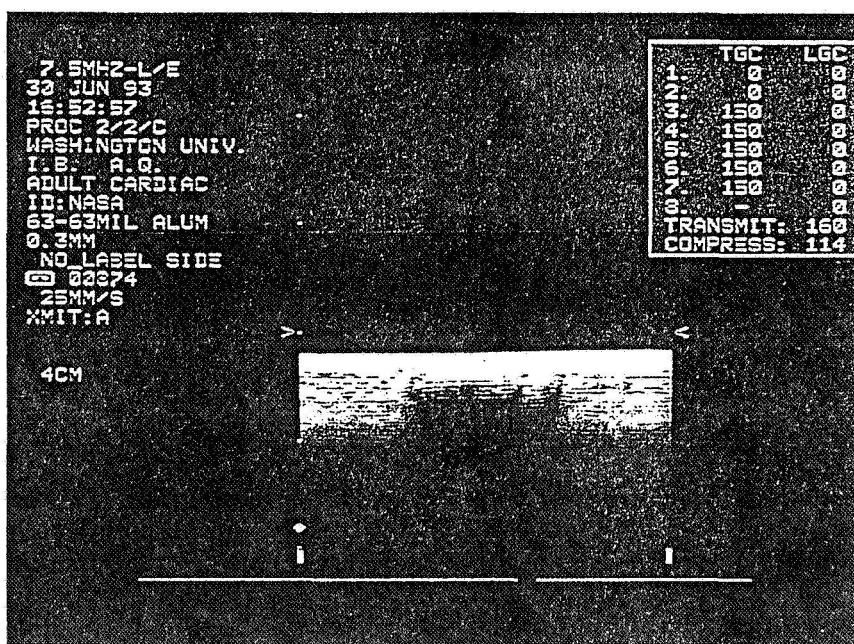
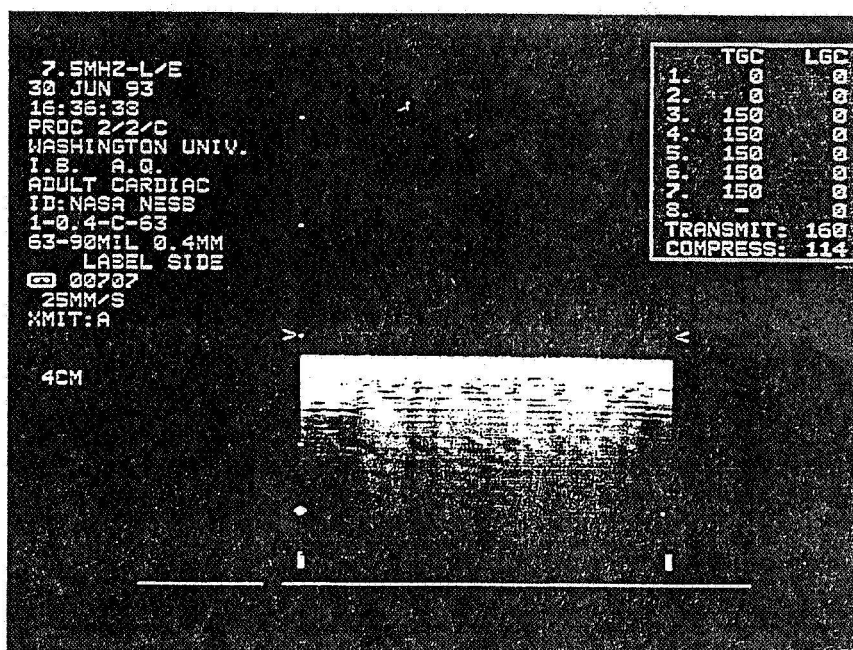


**Figure 4:** Linear array images over the disbonded region for specimen #1. Figure 4a shows the B-scan image of the disbonded region obtained from the "bottom" side of the specimen. Figure 4b shows the B-scan image of the disbonded region obtained from the "top" side of the specimen.



a)



b)

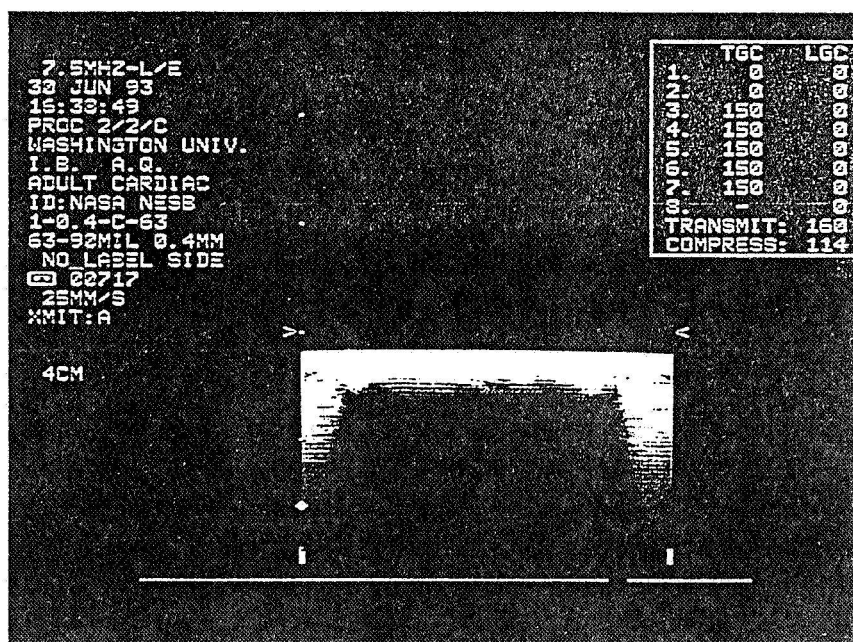


**Figure 5 :** Linear array images over the disbonded region for specimen #2. Figure 5a shows the B-scan image of the disbonded region obtained from the "bottom" side of the specimen. Figure 5b shows the B-scan image of the disbonded region obtained from the "top" side of the specimen.

### ***Contact Transducer Measurements***

In order to interpret the images of the bonded aluminum plate specimens obtained with the linear array, single element contact transducer measurements were performed. Ultrasonic rf A-lines from the bonded and disbonded regions of each specimen were obtained from each side of each specimen. Pulse-echo measurements were made with a broadband, 0.25-inch diameter, 25 MHz contact transducer (KB Aerotech - Alpha DFR) with a 0.98 cm (0.375 inch) delay line. A Panametrics 5800 computer controlled pulser/receiver was used to generate the broadband excitation pulse and to amplify the returned ultrasonic signal. The returned rf signal was taken from the Panametrics 5800 receiver output and sent to a Tektronix TDS 520 digitizing oscilloscope. Signals were digitized at a rate of 250 megasamples/second with 8-bit resolution over a total record length of 2500 points. The digitized rf signals were stored on a Macintosh IIfx for off-line analyses.

A set of at least three rf A-line signals were digitized from each region (bonded or disbonded) on each side ("bottom" or "top") of each specimen. The digitized signals of each set were very similar although small variations in signal size were observed. These small variations appear to be related to the variable degree of pressure one exerts when pressing the contact transducer on the surface of the specimen. Figure 6 depicts one representative rf A-line signal (amplitude) obtained from each of the specific areas of specimen #1. In this figure the rf A-lines representing the bonded region from both sides of specimen #1 appear to be very similar. This is consistent with the images in Figure 4 above and is a result of the inherent symmetry of this bonded aluminum plate specimen. There appears to be a modulation of the echo amplitudes in the rf A-line from the well-bonded region obtained from both sides of the specimen. This modulation may be the result of interference between signals returning from the various interfaces for the particular aluminum plate thickness and epoxy bond thickness of this specimen. These A-lines from the well-bonded regions show a significant amount of signal between the larger interface echoes that are due to multiple reverberations within the specimen.

Figure 6 shows that the amplitude echo decay pattern from the disbonded region of the "bottom" side of specimen #1 has a different shape than the rf A-lines obtained from the well-bonded region. The echo amplitudes from the disbonded region appear to decrease monotonically in time. Time between interface echoes in this region is approximately 0.50  $\mu$ sec, which corresponds to a round-trip distance of 0.32 cm in aluminum, twice the thickness of the bottom aluminum plate. Furthermore, it appears that there is not as much backscattered signal occurring between the interface echoes, suggesting that sound does not propagate easily beyond

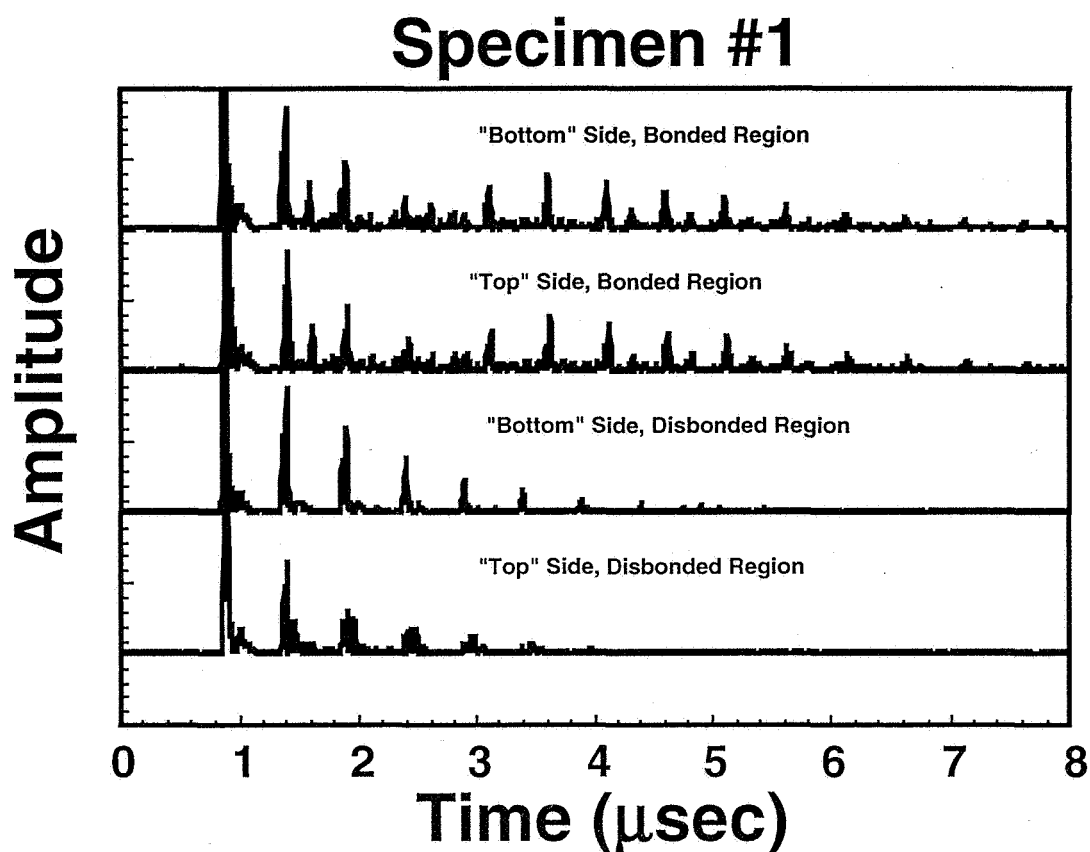


**Figure 6:** Representative rf A-line amplitude signals obtained from each of the specific regions of specimen #1.

the aluminum-tape interface from this side. The echo decay pattern from the disbonded region of specimen #1 obtained from the "top" side is also shown in Figure 6. This echo decay pattern demonstrates an apparent monotonic decrease in echo amplitude with time and it appears that this decrease in amplitude is at a greater rate than that observed for the disbonded region when measured from the "bottom" side. This A-line, obtained from the disbonded region of the "top" side, appears to have a significant amount of signal after the larger interface echoes. We hypothesize that the observed differences between the rf A-lines obtained from the disbond region of the "top" plate and the rf A-lines obtained from the disbond region of the "bottom" plate may be a consequence of the specific nature of the disbond/aluminum interfaces occurring at the "top" and "bottom" plates.

Figure 7 depicts the corresponding representative rf A-line signals (amplitude) obtained from each of the specific areas of specimen #2. The echo decay patterns for the well-bonded region from the two sides of the specimen ("bottom" and "top") do not appear to be the same as

they did for specimen #1. This is to be expected because the "bottom" and "top" aluminum plates are of different thicknesses for specimen #2 and the ultrasound propagates through the different layers of the specimen in a different sequence. The rf A-lines from this well-bonded region of specimen #2 do not appear to demonstrate such a strong modulation of the echo amplitudes with time. These A-lines show a significant amount of signal between the larger interface echoes, similar to that observed for specimen #1, which is due to multiple reverberations within the specimen.

As was observed for specimen #1, Figure 7 shows that the amplitude echo decay pattern from the disbonded region of the "bottom" side of specimen #2 has a different shape than that observed for the well-bonded region. The echo amplitudes from the disbonded region appear to decrease monotonically in time for specimen #2 as they did for specimen #1. Measurement of the time between interface echoes in this region provides a round-trip time of approximately 0.72  $\mu$ sec, which corresponds to a round-trip distance of 0.45 cm in aluminum, twice the thickness of the "bottom" aluminum plate of specimen #2. Furthermore, as was observed for specimen #1, it appears that there is not as much signal occurring between the interface echoes, suggesting that sound does not propagate easily beyond the aluminum-tape interface from this side. The echo decay pattern from the disbonded region of specimen #2 obtained from the "top" side is also shown in Figure 7. As found for specimen #1, this echo decay pattern also appears to demonstrate a decrease in signal amplitude at a greater rate than that observed for the disbonded region when measured from the "bottom" side. Again this is indicative of a greater attenuation of the signal and may be related to the specific nature of the aluminum/disbond interface. As was observed in specimen #1, there appears to be a significant amount of scattered signal after the larger interface echoes when compared with the signal obtained from the "bottom" side.

### *Discussion*

The results presented above, showing the images of the bonded aluminum plate specimens obtained with the linear array and the corresponding ultrasonic rf A-lines obtained with a contact transducer, suggest that linear array imaging can play a useful role in detecting disbonded regions and providing information describing bond interface characteristics. The disbonded region was easily discernible from the well-bonded region in the images obtained from either side of each specimen. Images of both specimens show that the disbonded region looks much different than the surrounding well-bonded region when the images obtained from the "bottom" of the specimen are compared with those obtained from the "top". The relatively

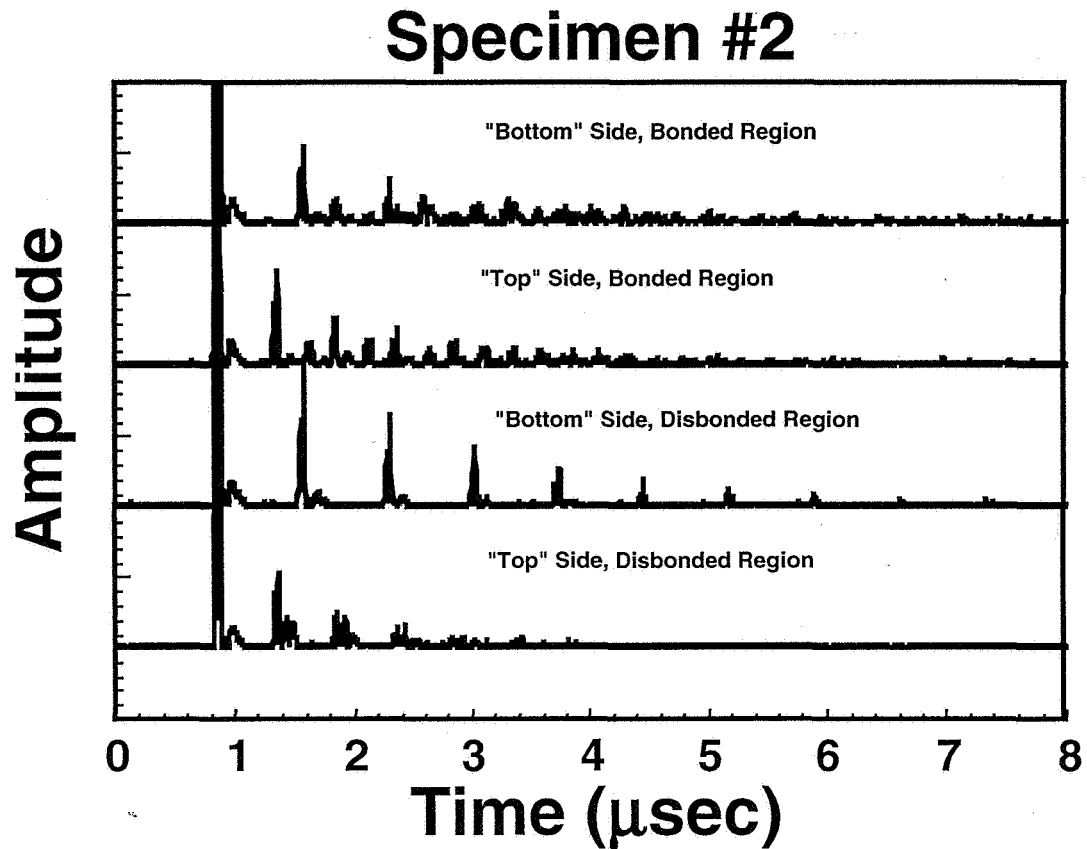


**Figure 7:** Representative rf A-line amplitude signals obtained from each of the specific regions of specimen #2.

"bright" disbond region observed when the specimens are imaged from the "bottom" side and the "dark" disbond region observed when the specimens are imaged from the "top" side agree with the corresponding echo decay patterns obtained with the contact transducer; i.e., a relatively higher attenuation associated with the disbonded region when interrogated from the "top" when compared with the results obtained from the "bottom". Subsequent destructive analysis of the specimens showed that the "bottom" plate was in direct contact with the adhesive of the masking tape (as expected) but the "top" plate had a thin substance adhered to it. These results suggest that the images obtained with the linear array may convey information regarding the characteristics of the interface between the aluminum and the disbond.

Images of the well-bonded regions of both specimens obtained with the SONOS 1500 linear array are also consistent with the contact transducer data. The modulation of the brightness of the well-bonded region in the images of specimen #1 agree well with the observed modulations in the echo decay patterns obtained with the contact transducer and the similarity

between the images of the bonded region from both sides of specimen #1 are consistent with the similar nature of the echo decay patterns from both sides. Images of specimen #2, which has aluminum plates of different thicknesses, are also consistent with the measured rf A-lines of this specimen. Images of specimen #2 show that the well-bonded region appears different when interrogated from the "bottom" side and compared with the image from the "top" side. This difference between the two sides is also evident in the measured echo decay patterns obtained from the two sides. The relatively longer echo decay pattern (lower attenuation) corresponding to the disbonded region of the "bottom" side of specimen #2 compared to the well-bonded region is also very evident in the image of that side.

The images of the bonded aluminum plate specimens and the corresponding agreement with contact transducer measurements suggest that linear array technology may provide a viable means to detect disbonded regions in bonded aluminum joints. Furthermore, these images may provide useful information regarding the nature of the disbonded region.

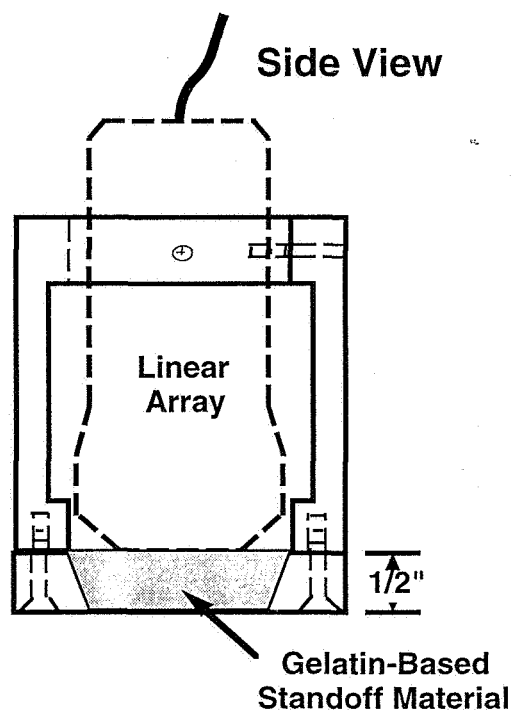


**Figure 8:** Standoff/delay fixture designed for use with the 7.5 MHz linear array probe.

*Standoff/Delay Fixture for the 7.5 MHz Linear Array*

In order to facilitate the inspection of specimens with the Hewlett-Packard SONOS 1500 medical imaging system a standoff/delay fixture was designed for use with the 7.5 MHz linear array probe. This standoff/delay fixture, illustrated in Figure 8, clamps around the Hewlett-Packard linear array probe. The use of the standoff/delay fixture in the inspection of the test specimens allows the specimen to be placed in a region away from the face of the linear array and thus reduces the effects of transducer ring-down and near field artifact. This is especially important when investigating relatively thin specimens with relatively large inherent ultrasonic velocities (compared to tissue). Furthermore, the use of this standoff/delay fixture allows the operator to keep the linear array probe perpendicular to the specimen under interrogation as the array is translated across the surface. The clamping screws allow precise alignment of the probe with respect to the surface. The standoff/delay material was a NASA developed, gelatin-based, tissue-mimicking material, with a velocity of sound close to that of tissue.<sup>12</sup>

#### IV. Comparison of Disbond Images

In this section, we describe the interrogation of three distinct types of adhesively-bonded aluminum plate specimens. The first type of specimen was a bonded-aluminum plate with a simulated disbond that spanned the entire bond thickness between the aluminum plates (complete disbond). The construction of this specimen is described in Section III of this Progress Report. The specimen had an total epoxy bond thickness of 0.03 cm and the width of the disbanded region was 1.27 cm . The measured total thicknesses of the entire specimen was 0.347 cm. Figure 9(a) illustrates the construction of this specimen with the complete disbond.

A second type of adhesively-bonded aluminum plate specimen interrogated was a specimen with a localized disbond. This specimen was also constructed using two identical aluminum plates of 0.16 cm in thickness with an area simulating a locally disbanded region. This bonded plate specimen was produced by layering one piece of adhesive tape over one piece of 0.004-inch (0.010 cm) thick paper in a specific area on one of the plates (referred to as the "bottom" plate). Epoxy was applied to the entire "bottom" plate which had the localized disbond and the "top" aluminum plate was applied. The specimen had an total epoxy bond thickness of 0.05 cm and the width of the locally disbanded region was approximately 1.91 cm (paper width was approximately 1.27 cm, adhesive tape width was approximately 1.91 cm). The mean measured total thicknesses of the entire specimen was 0.358 cm. Figure 9(b) illustrates the construction of this specimen with the localized disbond.

The third type of bonded aluminum plate specimen interrogated, was a bonded aluminum plate specimen with a series of flat-bottom holes backfilled with Styrofoam. This specimen consisted of 0.13 cm thick aluminum plates adhesively bonded together with type PR-1422 sealant obtained from Trans-World Airlines. The "bottom" aluminum plate had four regions of simulated corrosion consisting of 0.065 cm deep flat-bottom holes with diameters of 2.54cm (1-inch), 1.27cm (1/2-inch), 0.64cm (1/4-inch), and 0.32cm (1/8-inch), all backfilled with Styrofoam. Figure 9(c) illustrates the construction of this specimen with the Styrofoam-filled flat-bottom holes.

#### *Method of Linear Array Imaging*

Images of the specimens presented below were obtained using an unmodified, commercially-available Hewlett-Packard SONOS 1500 medical imaging system. Because these specimens were relatively thin, the SONOS 1500 imaging system was operated in a mode normally used to image specific peripheral blood vessels. Unfortunately, it was not possible to



change the depth setting of the images to correspond more closely to the thickness dimensions of the specimens. Furthermore, because the thicknesses of the specimens were relatively small and the velocity of sound in aluminum and carbon/epoxy is relatively large (compared to that of tissue), the images obtained with the SONOS 1500 system represent the echo-decay patterns of many round-trip echoes in the plates.

Images were obtained using a nominal 7.5 MHz center-frequency linear array probe with an overall length of 3.9 cm (1.5 inches). Each aluminum plate specimen was imaged using the gelatin-based stand-off described in Section III. The gelatin stand-off was implemented to bring the front surface echo of the specimens closer to the center of the image. The SONOS 1500 imaging system was configured such that the transmit power level was kept constant for all measurements and the same depth dependent gain (time-gain compensation) was applied to all depth segments. Video compression was adjusted to optimize the image contrast for each specimen interrogated. For the adhesively-bonded aluminum specimens, the disbonded region and surrounding regions of each specimen were imaged from both sides of the specimen; i.e., each specimen was imaged from the "bottom" side as well as the "top" side.

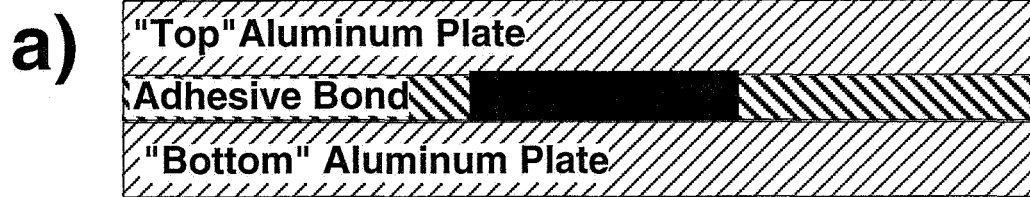
### ***Results of Linear Array Imaging***

In this section we present the resultant linear array images corresponding to the interrogation of the four types of specimens described above. The video images were presented on an accompanying videotape delivered to NASA Langley with our 9/94 Progress Report.

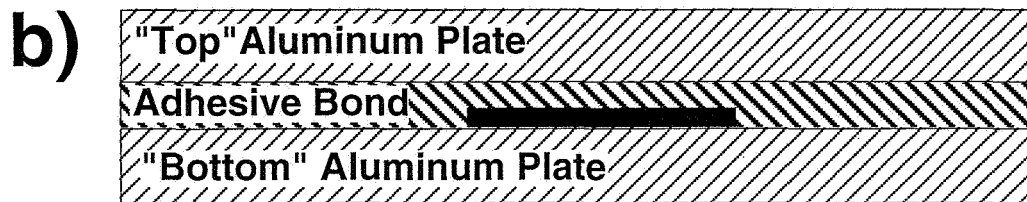
#### ***Adhesively-Bonded Aluminum with Complete Disbond***

The first set of images are of the bonded aluminum plates containing the complete disbond spanning the entire bond thickness between the "top" and "bottom" aluminum plates. In the first segment of videotape, the images obtained from the "bottom" side of the specimen where the masking tape was adhered to the aluminum plate are presented. The region of disbond can be readily distinguished from the surrounding well-bonded region in these images. These B-scan images represent the returned signals from many round-trip echoes (reverberations) inside the specimen which produce an entirely different echo decay pattern corresponding to the disbonded region when compared to the well-bonded region. The echo decay pattern corresponding to the disbonded region appears "brighter" than the surrounding regions and appears to monotonically decrease in brightness as time increases. Furthermore, the individual echo patterns do not appear as prominent in the disbond region as those observed in the surrounding regions thus giving the disbond region a more "smooth" appearance. The brightness

### Complete Disbond Specimen:



### Localized Disbond Specimen:



### Flat-Bottom Hole Specimen:

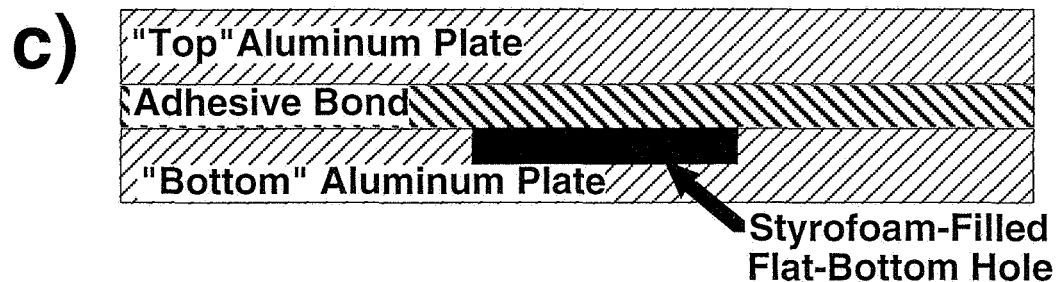


**Figure 9:** Diagram illustrating the three types of bonded-aluminum specimens interrogated: (a) complete disbond specimen, (b) localized disbond specimen, and (c) styrofoam-filled, flat-bottom hole specimen.

of the echo pattern from the well-bonded region appears to be more modulated and the individual echoes appear more prominently. The vertical dark lines which periodically appear in the images are probably the result of air bubbles present at the surface interface between the gelatin standoff and the specimen. These air bubbles at the surface "shadow" the ultrasound producing the dark lines.

In the second segment of videotape, the same specimen is interrogated from the "top" side. Again, the region of disbond can again be clearly distinguished from the surrounding well-

bonded region although it appears quite different than that observed when imaged from the "bottom" side of the specimen. The disbonded region appears to be much darker than the surrounding well-bonded regions when imaged from the "top". This appears to be indicative of a higher attenuation of ultrasound in the disbond region and hence a more rapid rate of echo decay when imaged from the "top" side. Although the disbond region looks very different when the images obtained from the "top" and "bottom" are compared, the well-bonded regions appear to be very similar in the two images. We would expect the images from the well-bonded regions to be very similar when imaged from both sides of the specimen because the thickness of each of the aluminum plates is the same and hence the ultrasound propagates along the same path in both cases. Figure 10 shows still-frame linear array images of this specimen obtained from both sides.

#### ***Adhesively-Bonded Aluminum with Localized Disbond***

Images in the next segment of videotape show the bonded aluminum plate specimen with a localized disbond. In the first set of images the specimen is interrogated from the "top" side. In this case ultrasound must propagate through the "top" aluminum plate and through the adhesive bond before encountering the disbonded region. The disbonded region can be readily discerned when the linear array is positioned such that both the well-bonded and disbond regions are visible simultaneously, although the image of the disbond is significantly different than that observed for the complete disbond as described above. The localized disbonded region appears as a "distorted" echo decay pattern and does not have the more uniform appearance of the of the complete disbond presented above.

In the next segment of videotape the linear array is used to image the localized disbond specimen from the "bottom" aluminum plate. In this case the interrogating ultrasound encounters the localized disbond before traversing the entire adhesive bond. Images of the localized disbond obtained from the "bottom" side are significantly different than that obtained from the "top" side. Images over the disbonded region show the echo decay pattern to persist significantly longer and appear somewhat "brighter" compared with the well-bonded region when imaged from the "bottom". This suggests that the reverberated ultrasound encounters less attenuation as the ultrasonic signals are "ringing" in the bottom plate and are not propagating into the adhesive bond. Figure 11 shows still-frame linear array images of this specimen obtained from both sides.

#### ***Adhesively-Bonded Aluminum with Styrofoam-Filled Flat-Bottom Holes***

In the next segment of videotape we show the linear array images obtained from the third type of specimen in which the "bottom" aluminum plate has Styrofoam-filled flat-bottom holes.

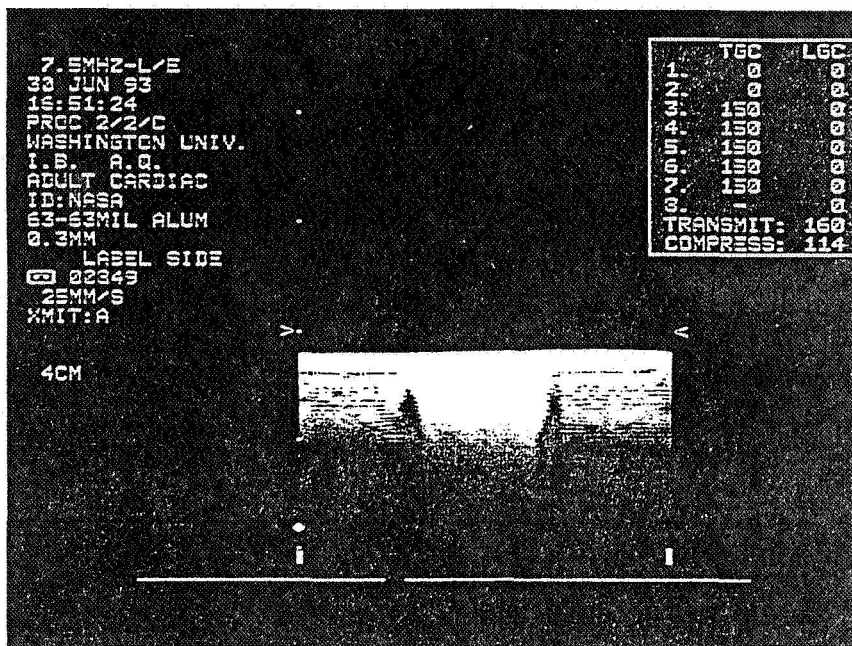
As described above, this specimen has four holes: 1-inch in diameter, 1/2-inch in diameter, 1/4-inch in diameter, and 1/8-inch in diameter. In the first set of images, the specimen was interrogated from the "top" side. In this case the ultrasound was transmitted through the "top" aluminum plate and transverses the entire adhesive bond before encountering the Styrofoam-filled flat-bottom holes. In the initial segment of videotape the linear array is placed over the 1/8-inch diameter flat-bottom hole. In this configuration, imaging from the "top" side, the 1/8-inch diameter flat-bottom hole is relatively difficult to see. Subsequent videotape segments showing the images of the regions corresponding to the 1/4-inch diameter, 1/2-inch diameter, and 1-inch diameter flat-bottom holes are also somewhat difficult to interpret and the effects of the Styrofoam-filled flat-bottom holes on the images are subtle.

In the next segment of videotape, the specimen is interrogated from the "bottom" side. In this configuration, the ultrasound encounters the flat-bottom hole prior to traversing the adhesive bond. In this case we obtain a much different image of the Styrofoam-filled flat-bottom holes. Here the position of the flat-bottom holes are much easier to observe. Images of the 1-inch diameter flat-bottom hole appear dark when compared to the surrounding well-bonded region indicating a high degree of attenuation of the reverberating ultrasonic signals. Similar images are observed for the 1/2-inch diameter, 1/4-inch diameter, and 1/8-inch diameter flat bottom holes. Figure 12 shows still-frame linear array images of this specimen obtained from both sides.

### *Discussion*

The linear array images presented above of the bonded aluminum plate specimens and woven composite laminate suggest that linear array imaging can play a useful role in detecting disbonded regions and flaws in a variety of specimens with specific types of disbonds or flaws. In imaging the bonded aluminum specimens the disbonded region was easily discernible from the well-bonded region in the images in many of the cases although the degree of contrast between well-bonded and disbonded regions appears to depend upon which side of each specimen was interrogated. Images of the complete disbond specimen, presented above, show that the disbonded region is readily identified when the specimen is imaged from either side. When the complete disbond specimen is imaged from the "bottom" side the disbonded region appeared bright and had a relatively longer echo decay pattern when compared with the well-bonded region. This suggests that the ultrasound was not as attenuated in the disbonded region and may represent ringing in the "bottom" plate with relatively little energy leaking out into the bond. When this same specimen is imaged from the "top" side the disbonded region appears much darker than the well-bonded region. This seems to indicate that the ultrasound is being more highly attenuated in this case. Possible reasons for this observed difference are described

a)



b)

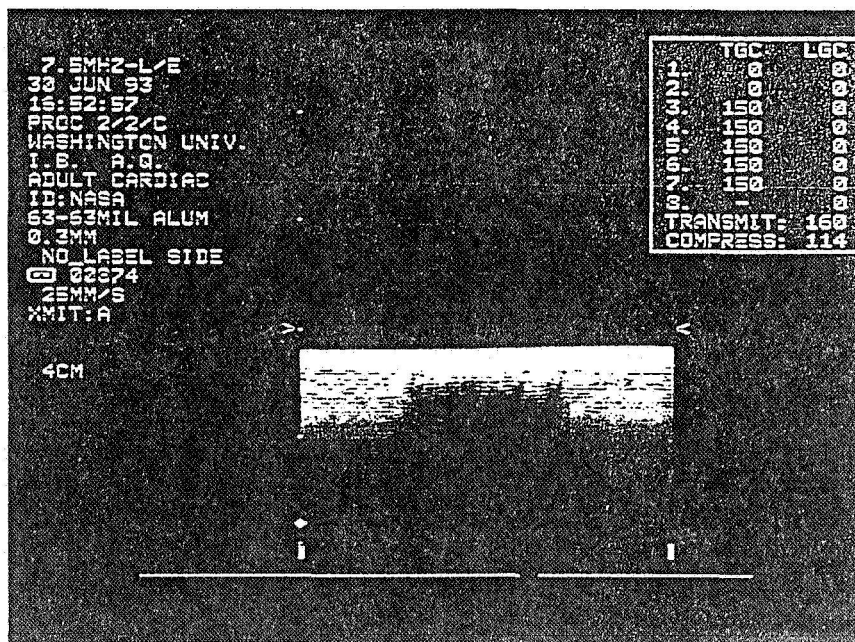
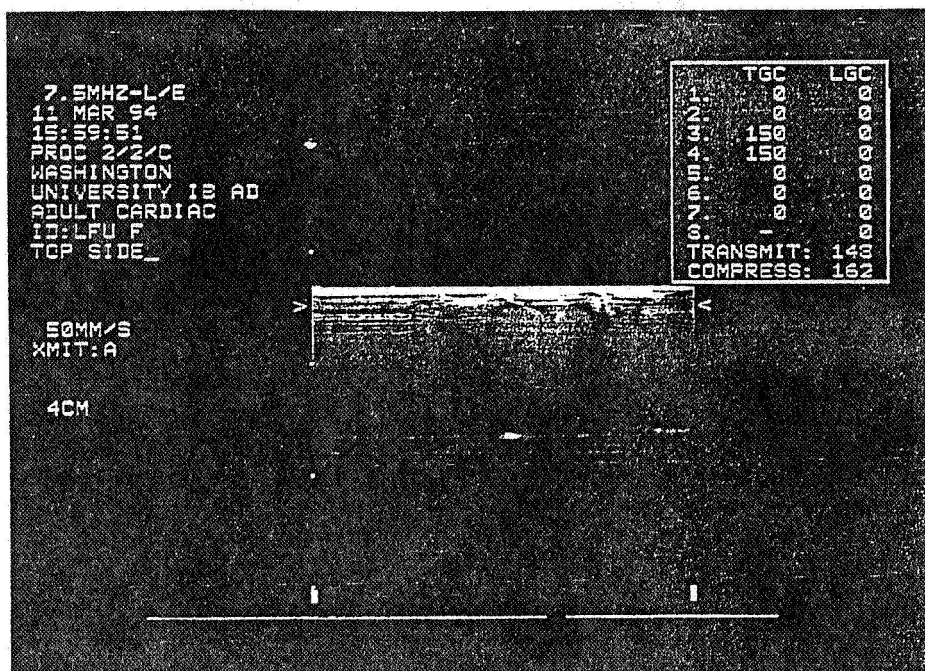


**Figure 10:** Linear array images over the disbonded region for complete disbond specimen. Figure 10a shows the B-scan image of the disbonded region obtained from the "bottom" side of the specimen. Figure 10b shows the B-scan image of the disbonded region obtained from the "top" side of the specimen.

a)



b)

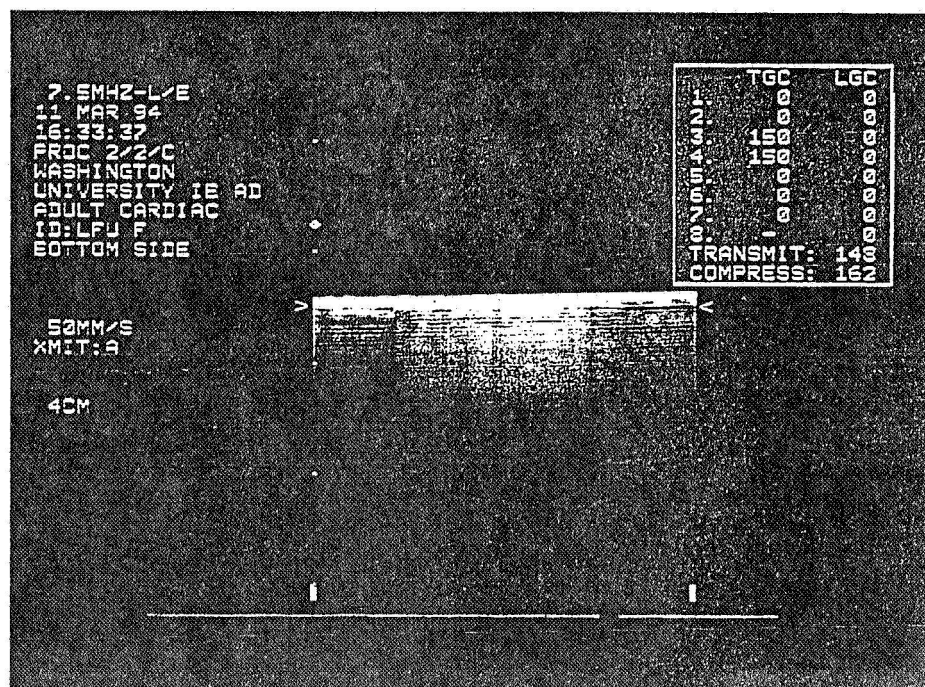
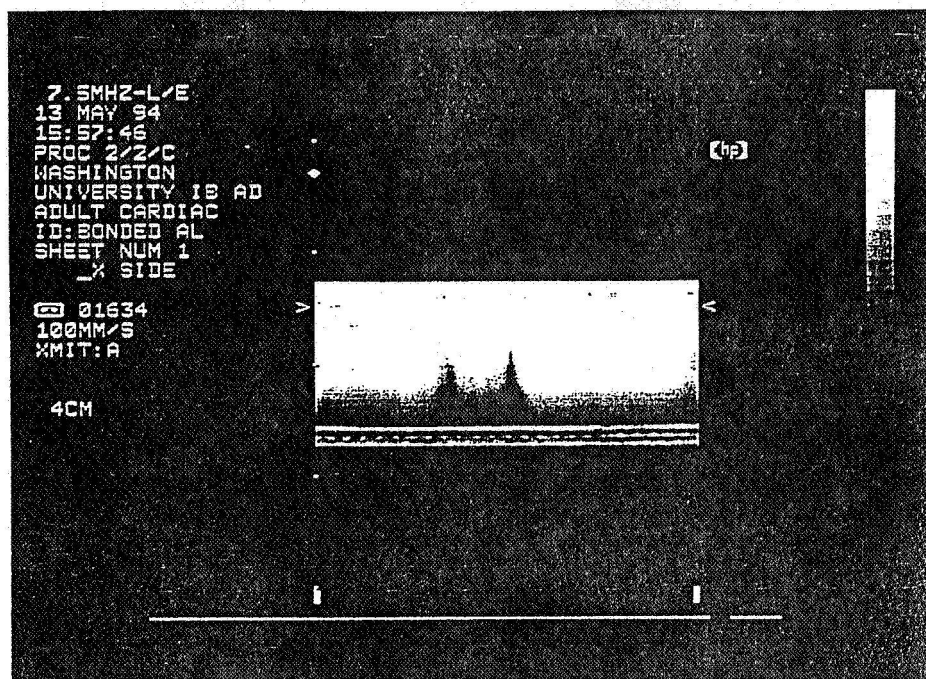


**Figure 11:** Linear array images over the disbonded region for the localized disbond specimen. Figure 11a shows the B-scan image of the disbonded region obtained from the "top" side of the specimen. Figure 11b shows the B-scan image of the disbonded region obtained from the "bottom" side of the specimen.



a)



b)

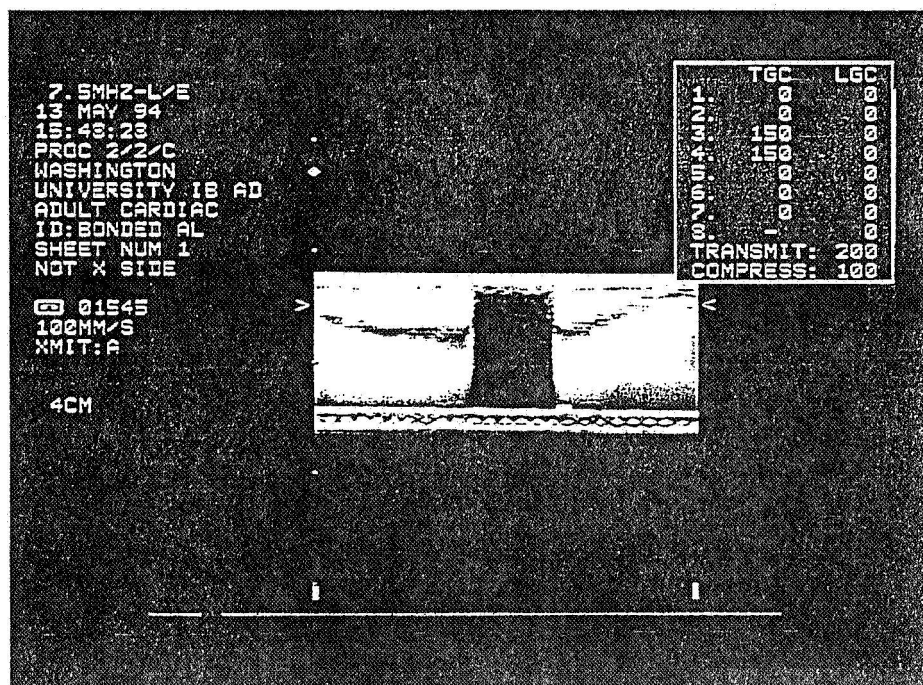


**Figure 12:** Linear array images over the disbonded region for styrofoam-filled flat-bottom hole specimen. Figure 12a shows the B-scan image of the disbonded region obtained from the "top" side of the specimen. Figure 12b shows the B-scan image of the disbonded region obtained from the "bottom" side of the specimen.

in Section III. The fact that there is a significant difference in the way the echo decay patterns are observed when the specimen is imaged from the two sides suggests that information regarding the interface between the disbond and the aluminum can be determined.

The images of the localized disbond specimen also show a significant difference in the observed echo decay pattern when the disbonded region is imaged from the two sides of the specimen. Images of the disbonded region obtained from the "top" side of the specimen show the echo decay pattern associated with the disbond region to be distinct from the well-bonded region but does not have a uniform echo decay pattern across the width of the disbonded region. This may be due to the fact that the ultrasound must traverse the entire bond thickness before encountering the disbond and the echo decay pattern consists of contributions arising from the "top" plate to bond interface and bond to localized disbond interface. Both of these contributions will combine to form a somewhat complex echo decay pattern. Images of the localized disbond obtained from the "bottom" side of the specimen show a significantly different echo decay pattern. In this case the echo decay pattern is more uniform and appears "brighter" than the surrounding well-bonded region. This observation seems to be consistent with what might be expected when the localized disbond is imaged from this side. One hypothesis is that the ultrasound is reverberating in the "bottom" plate and very little is being transferred through the localized disbond and into the bond region; hence resulting in the "bright", relatively non-attenuating echo-decay pattern.

The linear array images of the bonded-aluminum plate specimen with the Styrofoam-filled flat-bottom holes also show a significant difference between the images obtained from the "top" and "bottom" of the specimen. When imaged from the "top" plate the flat-bottom holes are very difficult to identify. In this case the ultrasound must traverse the entire bond thickness before encountering the Styrofoam-filled flat-bottom holes. Here, as with the localized disbond specimen when imaged from the "top" side, the resultant echo decay pattern is the result of a complex combination of interface echoes occurring at the "top" plate-adhesive bond and bond-Styrofoam interfaces. Apparently the acoustic impedance mismatch between the adhesive bond and Styrofoam is not significantly different than the impedance mismatch between the adhesive bond and aluminum and thus the observed echo decay pattern is not significantly altered. When this specimen is imaged from the "bottom" side the Styrofoam-filled flat-bottom holes are readily apparent. In this case the echo decay pattern associated with the flat-bottom holes shows up dark relative to the well-bonded region. One hypothesis might be that the ultrasound propagates through the "bottom" aluminum plate and into the Styrofoam where it is absorbed. Hence the



echo decay pattern is more highly attenuated and shows up dark relative to the well-bonded region.

### ***Conclusions***

These results suggest that the images obtained with the linear array may convey information regarding the characteristics, location, and interface properties of specific types of flaws in different materials and structures. Furthermore, linear array imaging may offer the advantage of being able to compare "good" regions with "flawed" regions simultaneously, and in real time. Observation of an image in real-time can offer the operator the ability to "interact" with the inspection process, thus providing new capabilities, and perhaps, new approaches to nondestructive inspections. This enhancement may aid in the probability of detection and real-time characterization of certain types of flaws.

## **V. Comparison of Linear Array Detection of Disbond Regions in Bonded Aluminum Plates With Contact Measurements (Analytic Signal)**

In this Section we present images of a bonded aluminum plate sample with a simulated disbond region. The disbond region was produced by adhering a piece of plain white paper to a piece of cellophane tape and applying the paper-tape combination to one of the aluminum plates. Because the area under the paper was not adhesively bonded to the aluminum plate we feel that this arrangement more closely simulates a disbond. Images are also presented for an aluminum plate sample with an epoxy strip adhered to one side to help provide information for the interpretation of the images of the bonded aluminum plate sample containing the disbond region. These images are compared with corresponding conventional ultrasonic contact transducer measurements in order to provide information regarding the nature of the disbonded region. We anticipate the results of this on-going investigation may provide a step toward the development of a rapid, real-time, and portable method of ultrasonic inspection and characterization based on linear array technology.

We describe the preparation of the aluminum plate specimens interrogated and the method of linear array imaging. Linear array images and results from contact transducer measurements are presented.

### ***Sample Preparation***

Two aluminum/epoxy samples were prepared for the investigation. One sample consisted of two aluminum plates bonded with epoxy which contained a region of simulated disbond. The other sample was a single plate of aluminum with a strip of epoxy adhered to one side.

### ***Bonded Aluminum Plate Sample (Sample F)***

The bonded aluminum plate sample (sample F) interrogated in this investigation was 2 1/4" wide by 3 9/16" in length. Two identical aluminum plates of 0.0615" in thickness were used in the production of sample F. The sample was constructed with an area of layered paper/cellophane tape to simulate a disbonded region. The bonded plate sample was produced by adhering a piece of plain white paper (0.0038" thick, 1/2" wide by 1 1/2" long) to a piece of cellophane tape (3/4" wide by 1 1/2" long). The paper-tape was applied to the "bottom" plate. "Duro Master Mend™" epoxy was applied to the "bottom" plate which had the paper/cellophane tape attached and a "top" aluminum plate was applied. Weights were applied to the sample to produce a constant compressive force during the cure process. After the epoxy had cured the

specimens were machined to their final length and width dimensions leaving only one area of simulated disbond. The final thickness of sample F was 0.141". Figure 13 illustrates how sample F was constructed.

### ***Single Plate of Aluminum With an Epoxy Strip (Sample E)***

In order to compare the effects on the reflected ultrasound at the aluminum/paper interface ("disbond") to the well-bonded regions of sample F, a single plate aluminum sample (sample E) was constructed with a strip of epoxy applied to one side. The aluminum plate was 3 9/16" in length by 2 1/8" wide and 0.0615" thick and the epoxy strip was 3/4" wide by 2 1/8" long. The measured total thickness of the resultant aluminum plus epoxy region was 0.0729". Figure 14 illustrates the construction of the aluminum/epoxy-strip sample.

### ***Method of Linear Array Imaging***

The aluminum plate samples were imaged with an unmodified Hewlett-Packard SONOS 1500 medical imaging system in the peripheral vascular imaging mode. A nominal 7.5 MHz center-frequency linear array probe was used with an overall length of 1.5 inches. Between the sample and the linear array probe a gelatin stand-off was employed as illustrated in Figure 15. The gelatin stand-off served to move the front surface echo of the aluminum specimens closer to the center of the image. Each sample was imaged with the axis of the linear array along the long axis (length dimension) of the sample so that the linear array straddled the disbond region. The transmit power level of the SONOS 1500 imaging system was kept constant and the same depth dependent gain (time-gain compensation) was applied to all depth segments for all the measurements. For each sample interrogated the video compression was adjusted to optimize the image contrast and remained constant.

The disbanded region and surrounding regions of sample F were imaged from both sides of the specimen; i.e., sample F was imaged from the aluminum plate side in contact with the paper-cellophane tape ("bottom" side) as well as on the opposite side ("top" side). Sample E was interrogated from the aluminum plate side of the sample.

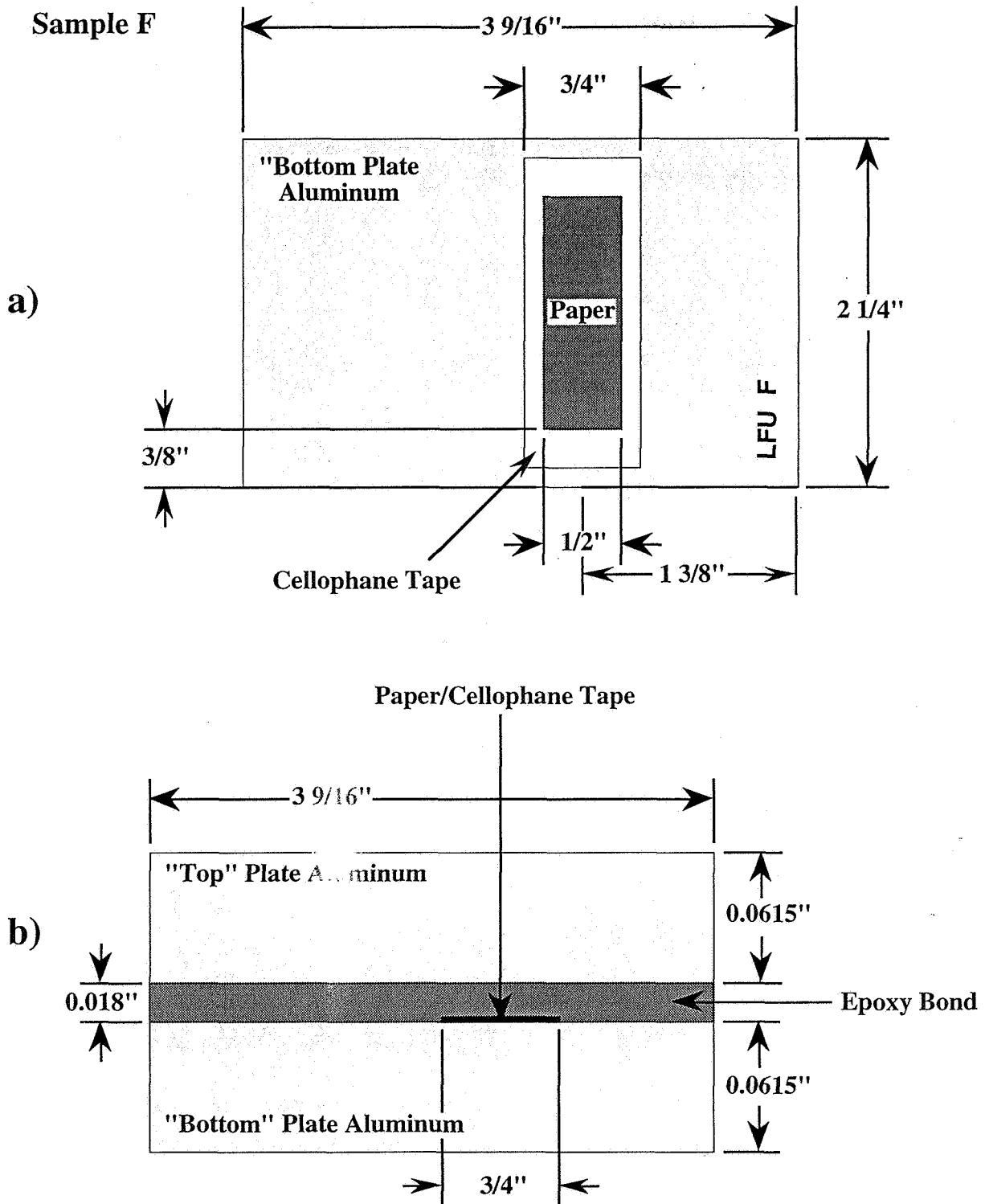
Figure 16 illustrates how to interpret the images presented of the samples obtained with the linear array system. For sample F the images were acquired with the linear array straddling the disbond region (imaged from the "top" plate side and the "bottom" plate side). For sample E, the aluminum plate plus the epoxy strip sample, the linear array insonified from the aluminum plate side of the sample straddling the epoxy strip. As discussed in Section III, these images are

composed of many reverberations of the ultrasonic signal in the sample and do not represent a single cross-sectional view. The general pattern seen in the images (as depicted in Figure 16) will be lightly shaded regions on either side of the disbond region for sample F and the epoxy strip region for sample E. The center portion of the image will display a characteristic reverberation pattern dependent on the type of interfaces encountered for the given sample. In the areas of the image representing the disbond region of sample F the exact shading of the reverberating signal will depend on the side of insonification.

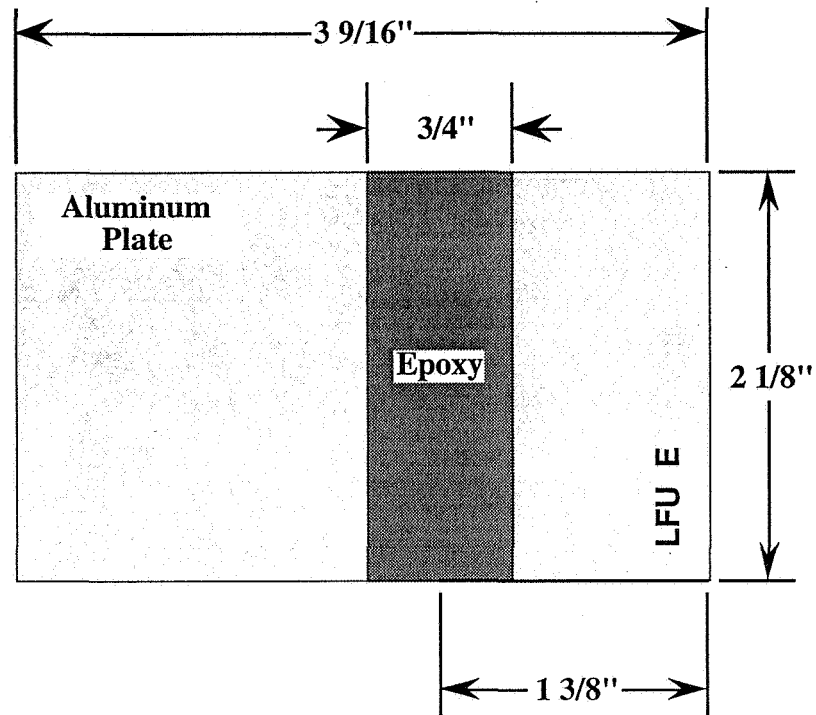
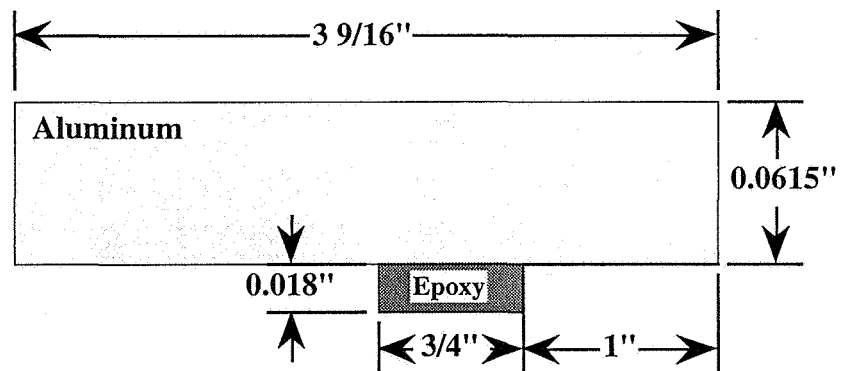
### ***Linear Array Images***

Figure 17 shows the linear array B-scan image over the epoxy region for the sample with the epoxy strip (sample E). The image was acquired by insonifying the aluminum plate side of the sample (opposite to the side with the epoxy strip). The strip of epoxy region is clearly distinguished from the aluminum plate only regions. The side regions which represent the aluminum/air interface display a reverberation decay pattern that appears bright and long in duration. This is to be expected because the aluminum to air interface presents a large acoustic impedance mismatch and a large portion of the acoustic energy is reflected at this interface. Because aluminum is a rather low-loss material, we see a bright and long decay pattern. The center portion of the image displays the area of the aluminum/epoxy interface. A smaller acoustic impedance mismatch is presented to the acoustic wave in this region and thus some acoustic energy travels into the epoxy region. Because epoxy is more attenuating than aluminum we see that the reverberation pattern appears to be less bright and shorter in duration than the surrounding side regions.

Figure 18 shows the linear array B-scan images over the disbonded region for sample F from both sides. In Figure 18a the image was acquired by insonifying the "bottom" side of the sample where the paper-tape was adhered to the aluminum plate. The region of the disbond can be clearly distinguished from the surrounding well-bonded region in this image. The aluminum/paper interface appears to present a greater acoustic impedance mismatch than the aluminum/epoxy regions on either side of the disbond region. Since epoxy is considerably more attenuating than aluminum, more acoustic energy is reflected at the aluminum/paper interface than at the aluminum/epoxy interface and we see a brighter and longer decay pattern. This decay pattern results from the reverberation of the acoustic energy in the "bottom" aluminum plate.



**Figure 13:** Illustration of the construction of the sample F (the bonded aluminum plate sample). a) Looking down on the "bottom" plate b) A cross-sectional representation, the horizontal dimension is to scale while the vertical dimension is exaggerated (x 3.4) for clarity.

**Sample E****a)****b)**

**Figure 14:** Illustration of the construction of the sample E (the aluminum plate with epoxy sample). a) Looking down on the aluminum plate b) A cross-sectional representation, the horizontal dimension is to scale while the vertical dimension is exaggerated (x 3.4) for clarity.

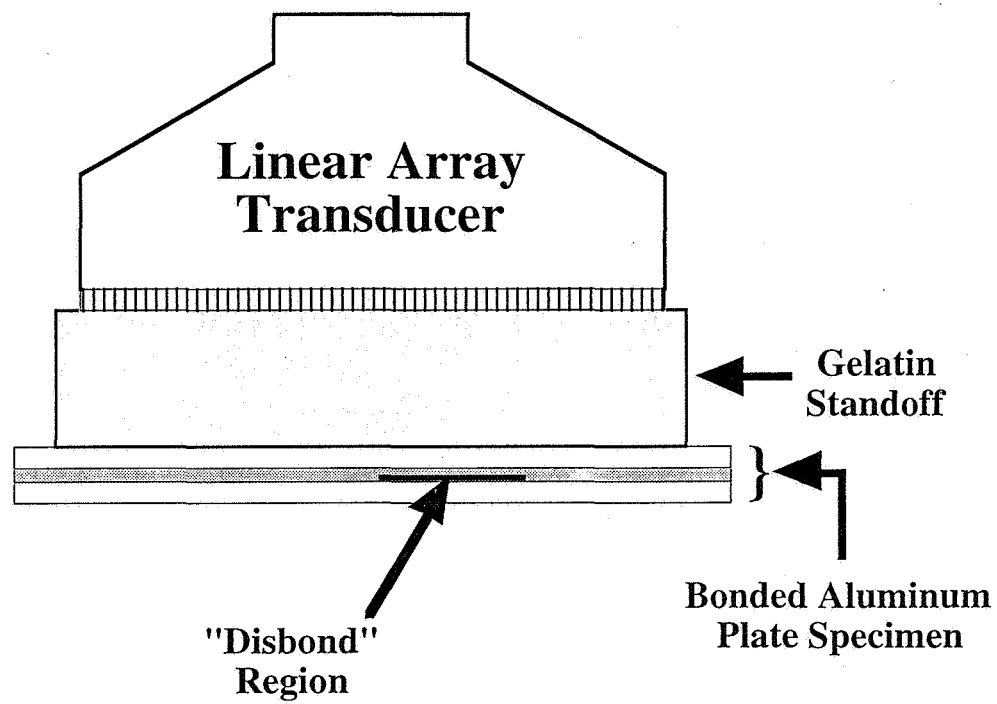


**Figure 15:** Configuration of linear array transducer and gelatin standoff for obtaining images of the samples.

## Cartoon Depicting Typical Linear Array Images

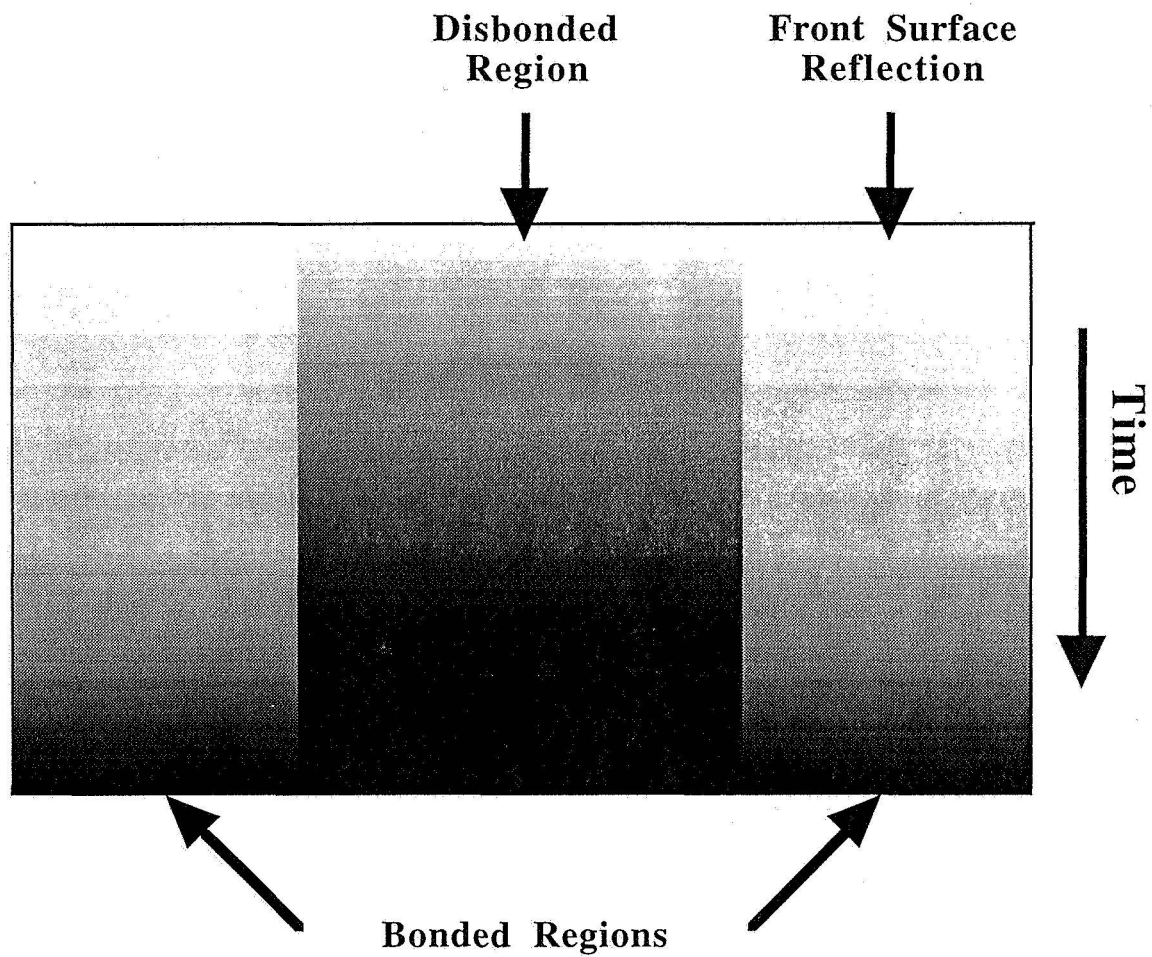


**Figure 16:** Cartoon illustrating how to interpret the linear array images.



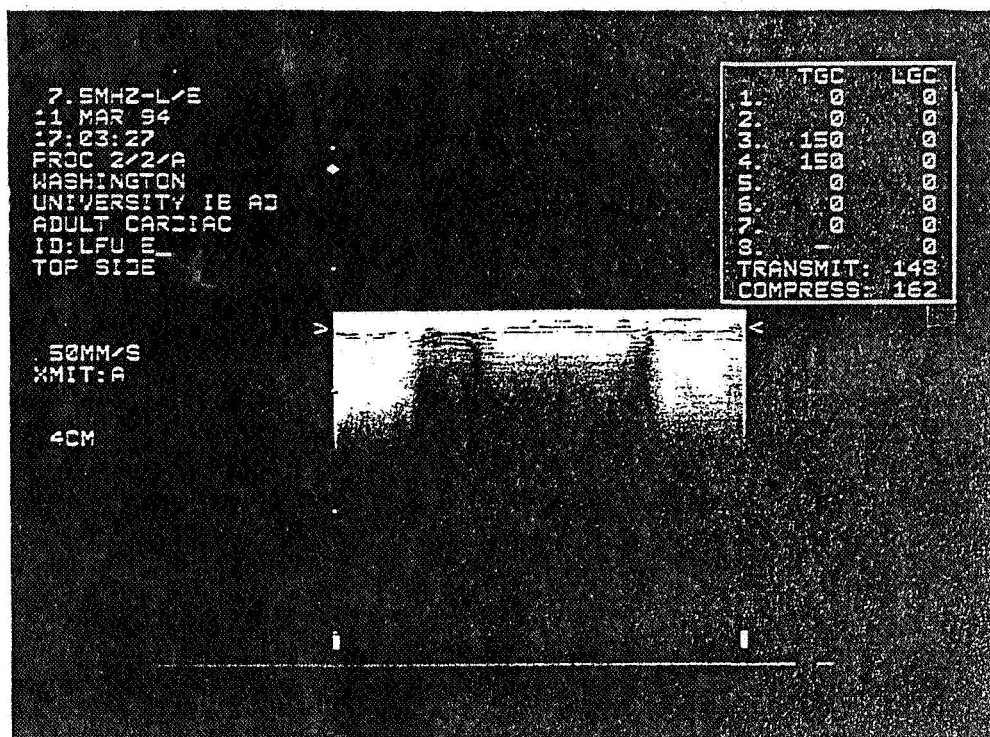


**Figure 17** - Linear array image over the epoxy strip region of sample E.

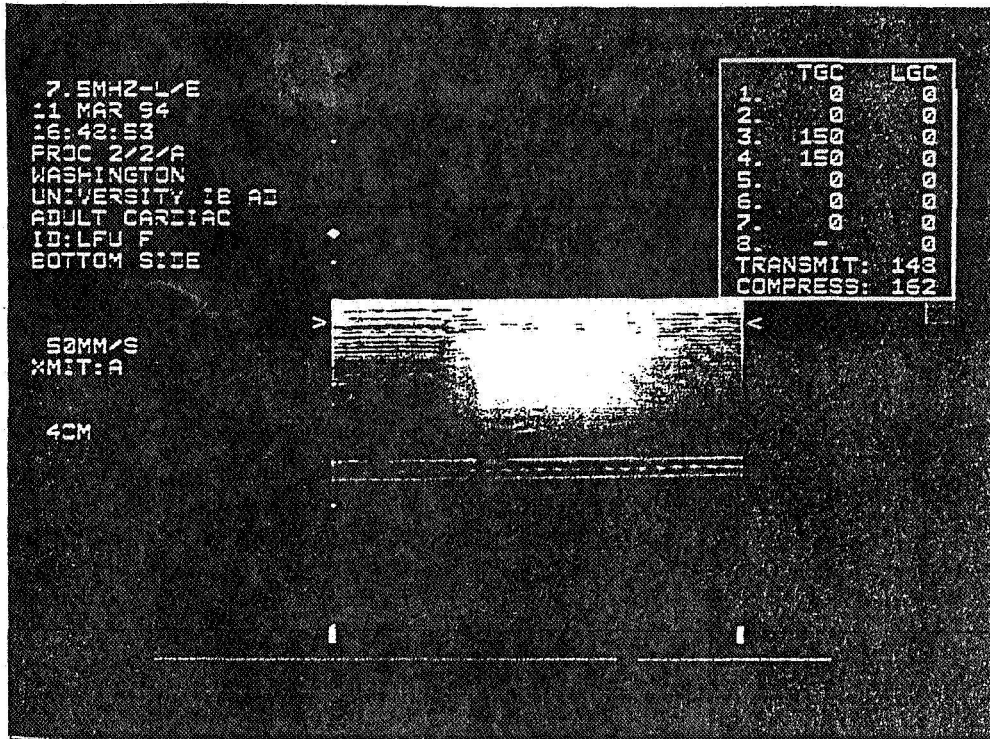
Figure 18b shows the B-scan image of the disbanded region of sample F obtained from the "top" side of the specimen. In this image the region of disbond can again be clearly distinguished from the surrounding well-bonded region although it appears different than that observed when imaged from the "bottom" side of the sample (Figure 18a). If we compare the center portion of the image of Figure 18b with the center portion of Figure 17, we see that the decay patterns display similar features. This is the same situation encountered when imaging the epoxy strip sample in sample E. Ultrasound propagates through the "top" aluminum plate and into the epoxy before encountering the air interface. Hence, the echo decay pattern observed for the sample over the disbond when imaged from the "top" side is similar to the image of the epoxy strip in sample E. This acoustic impedance mismatch reflects a large portion of the acoustic energy. The resultant decay pattern is dominated by the reverberation in the "top" aluminum plate and the epoxy layer. Because epoxy is more attenuating than aluminum the epoxy layer dampens the decay pattern. The well-bonded side regions (aluminum/epoxy/aluminum regions) appear to be very similar in the two images. We would expect the images from the well-bonded regions to be very similar when imaged from both sides of the sample because the thickness of each of the aluminum plates is the same and hence the ultrasound propagates along the same path in both cases.

### *Contact Transducer Measurements*

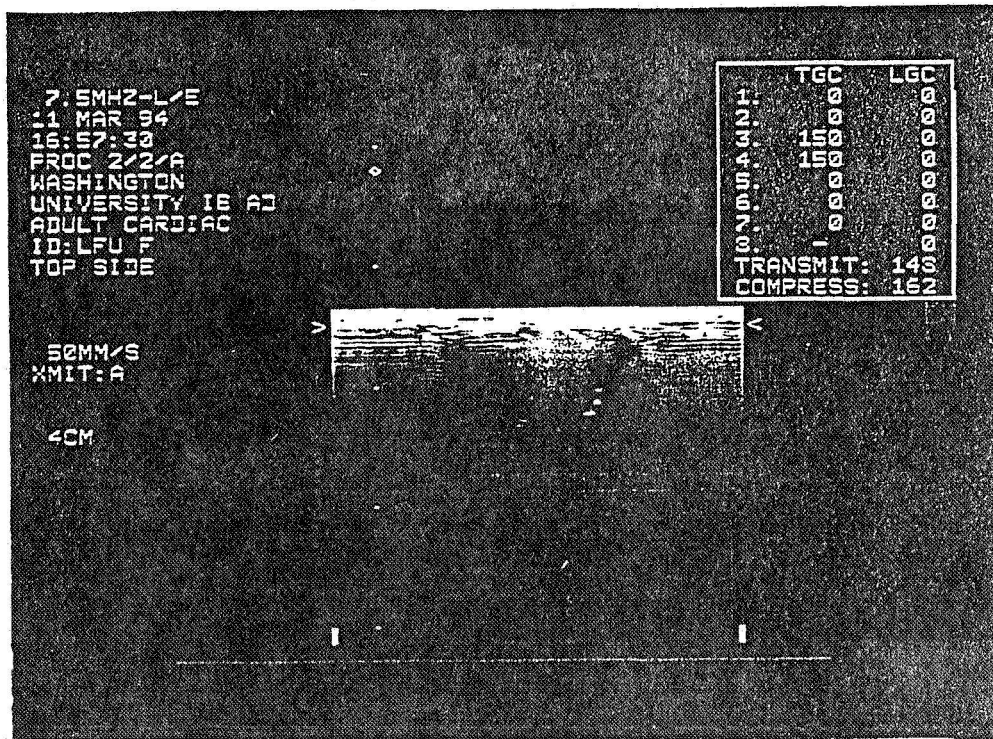
In order to substantiate the interpretations of the images of the aluminum plate specimens obtained with the linear array, single element contact transducer measurements were performed. Ultrasonic rf A-lines from the bonded and disbonded regions of sample F were obtained from each side of the specimen. For sample E the side opposite the epoxy strip was insonified. The rf A-lines from sample E were obtained from both the aluminum only area and the aluminum/epoxy area of the sample. Pulse-echo measurements were made with a broadband, 1/4" diameter, 25 MHz contact transducer (KB Aerotech - Alpha DFR) with a 3/8" delay line. A Metrotek MP215 pulser was used to generate the broadband excitation pulse and a MR106 receiver was employed to amplify the returned ultrasonic signal. The returned rf signal was taken from the MR106 receiver output and sent to a Tektronix TDS 520 digitizing oscilloscope. Signals were digitized at a rate of 250 megasamples/second with 8-bit resolution over a total record length of 2500 points. The digitized rf signals were stored on a Macintosh Quadra 840AV for off-line analyses.

In what follows all the figures displaying the signals obtained with the 25 MHz contact transducer will show both the rf and the magnitude of the analytic signal of the rf superimposed to help guide the eye to the encountered interfaces. Figure 19a displays the rf A-line acquired over the aluminum only portion of sample E. The velocity of sound for aluminum is about 6.35 mm/ $\mu$ sec which for a thickness of 0.0615" yields a round trip time (distance traveled is 2 times 0.0615") between reverberations of 0.492  $\mu$ sec. Figure 19b displays the ultrasonic signals over the aluminum/epoxy region of the sample. We see additional reflections inserted between the aluminum echoes. These reflections occur due to the epoxy to air interface. If we compare Figure 19a and 19b we see that the decay patterns decrease more rapidly for the aluminum/epoxy region than for the aluminum only region. As discussed above, this is what we would expect because the ultrasound that travels into the epoxy region decays more rapidly due to the higher attenuation of the epoxy as compared with aluminum. These reverberation decay patterns are responsible for the resultant decay patterns observed in the linear array image of sample E (see Figure 17).

Figures 20 and 21 display the rf A-lines obtained from the bonded aluminum plate sample (sample F). Figure 20a displays the rf and analytic signal for insonification of the "bottom" side in a well-bonded region of sample F. Figure 20b displays the signals when the sample was flipped over and insonified in the same region as Figure 20a but from the opposite side. We see that the signals in 20a and 20b appear to be quite similar. This is to be expected since the thickness of the two aluminum plates are equal.



a)



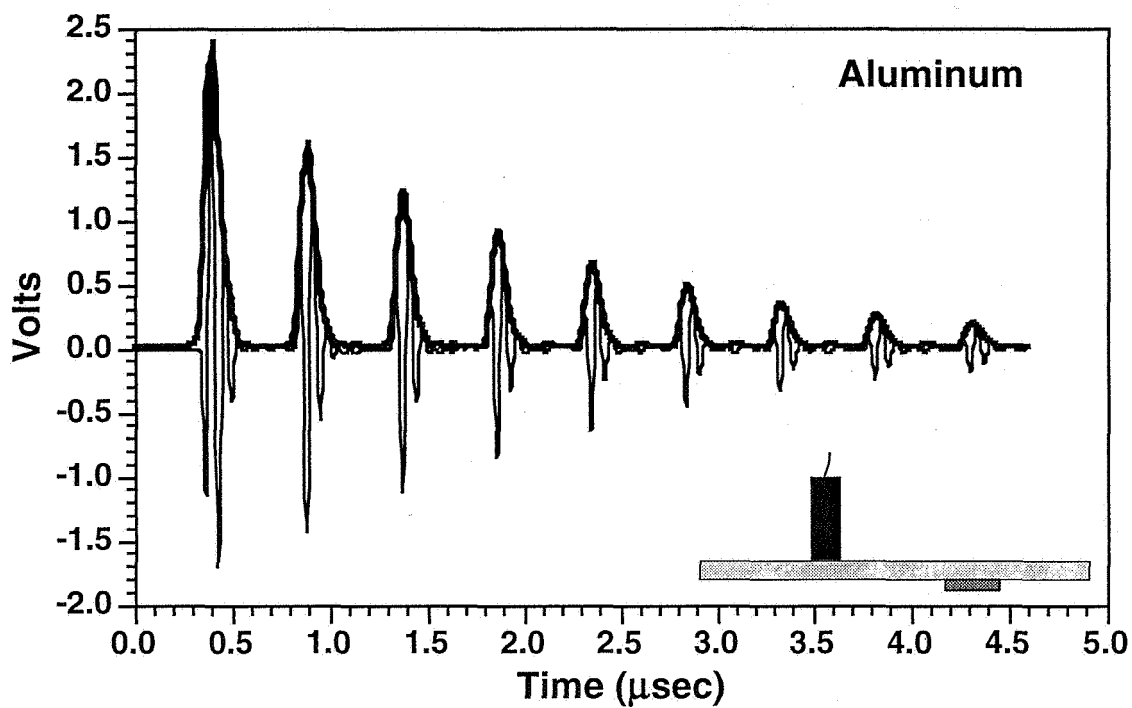
b)

**Figure 18:** Linear array images over the disbonded region for sample F. Figure 18a shows the B-scan image of the disbonded region obtained from the "bottom" side of the specimen. Figure 18b shows the B-scan image of the disbonded region obtained from the "top" side of the specimen.

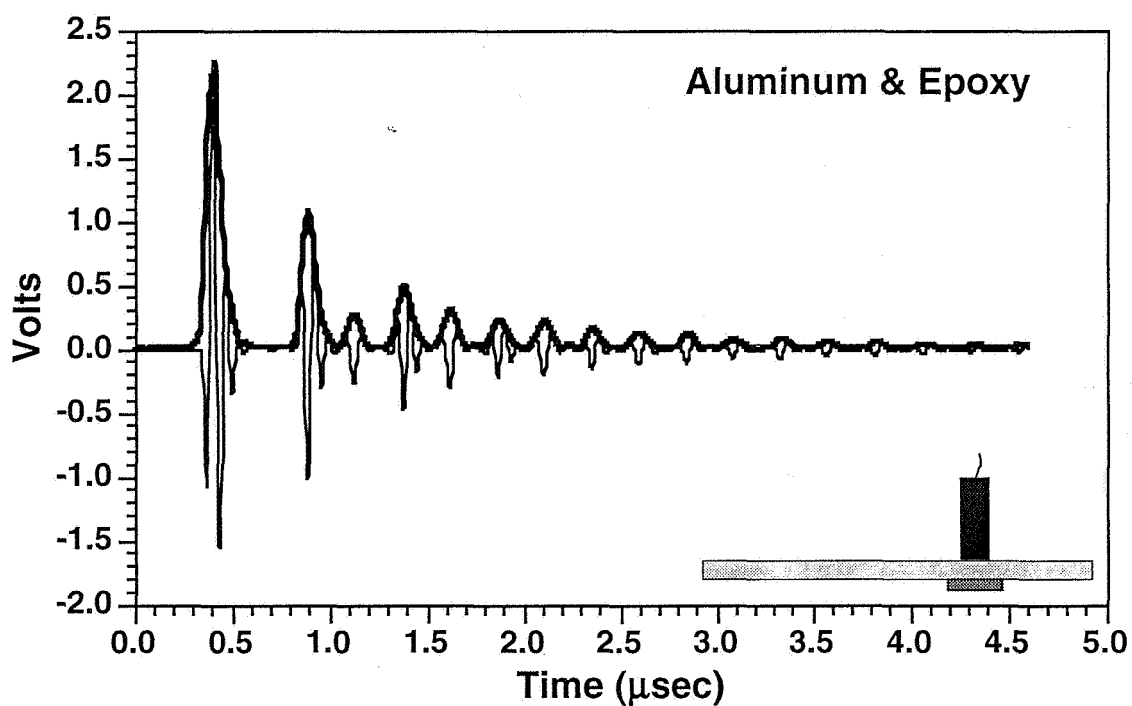
In Figure 21a sample F was insonified from the "bottom" side of the specimen (the side to which the paper-tape was applied) with the transducer positioned over the region of the disbond. Figure 21b displays the rf A-line and analytic signal for the same region except that the sample is insonified from the "top" side of the sample. The rf signal for insonification of the "top" side decays more rapidly than the rf obtained from insonifying the "bottom" side. As discussed above because epoxy is more attenuating than aluminum the epoxy layer dampens the decay pattern. If we compare Figure 21a with Figures 20a and 20b we see that they all appear very similar.

### *Discussion*

The results presented above, showing the images of the bonded aluminum plate specimen and the aluminum/epoxy-strip specimen obtained with the linear array and the corresponding ultrasonic rf A-lines obtained with a contact transducer, suggest that linear array imaging can perform a useful role in detecting disbanded regions and providing information describing bond interface characteristics. The disbanded region was easily discernible from the well-banded region in the images. The images also show that the disbanded region looks quite different from that of the surrounding well-banded region in sample F when the images obtained from the "bottom" of the specimen are compared with those obtained from the "top". The relatively "bright" disbond region observed when sample F was imaged from the "bottom" side and the "dark" disbond region observed when the sample was imaged from the "top" side agree with the corresponding echo decay patterns obtained with the contact transducer; i.e., a relatively higher attenuation associated with the disbanded region when interrogated from the "top" when compared with the results obtained from the "bottom".

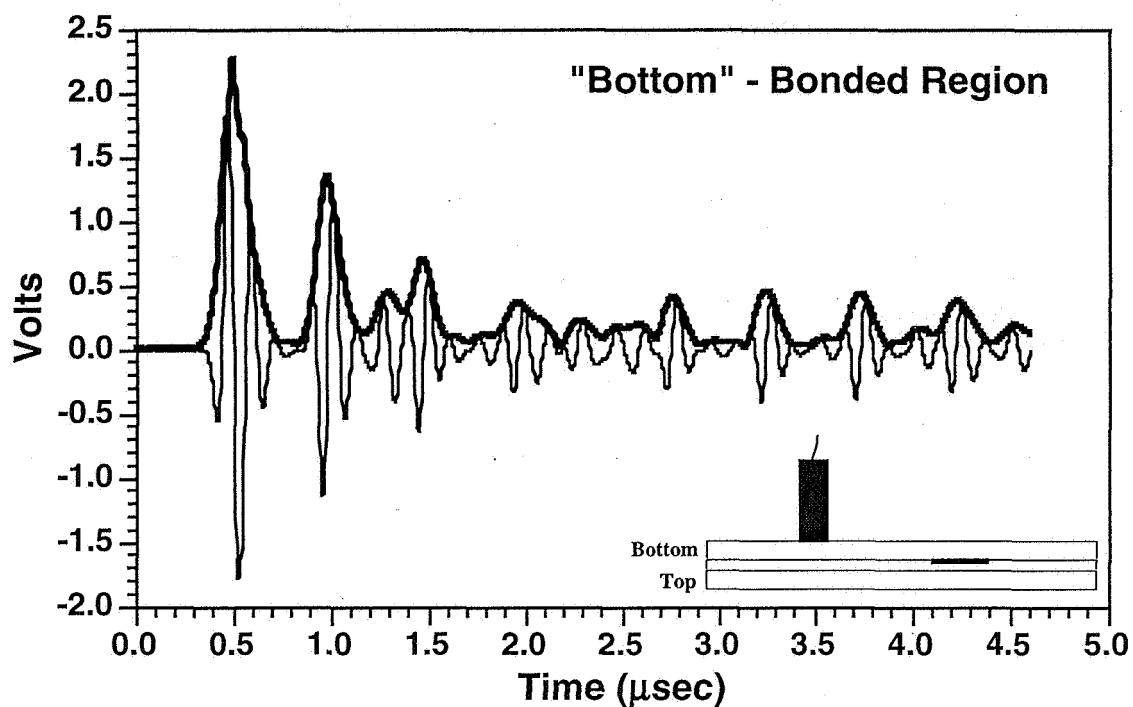


a)

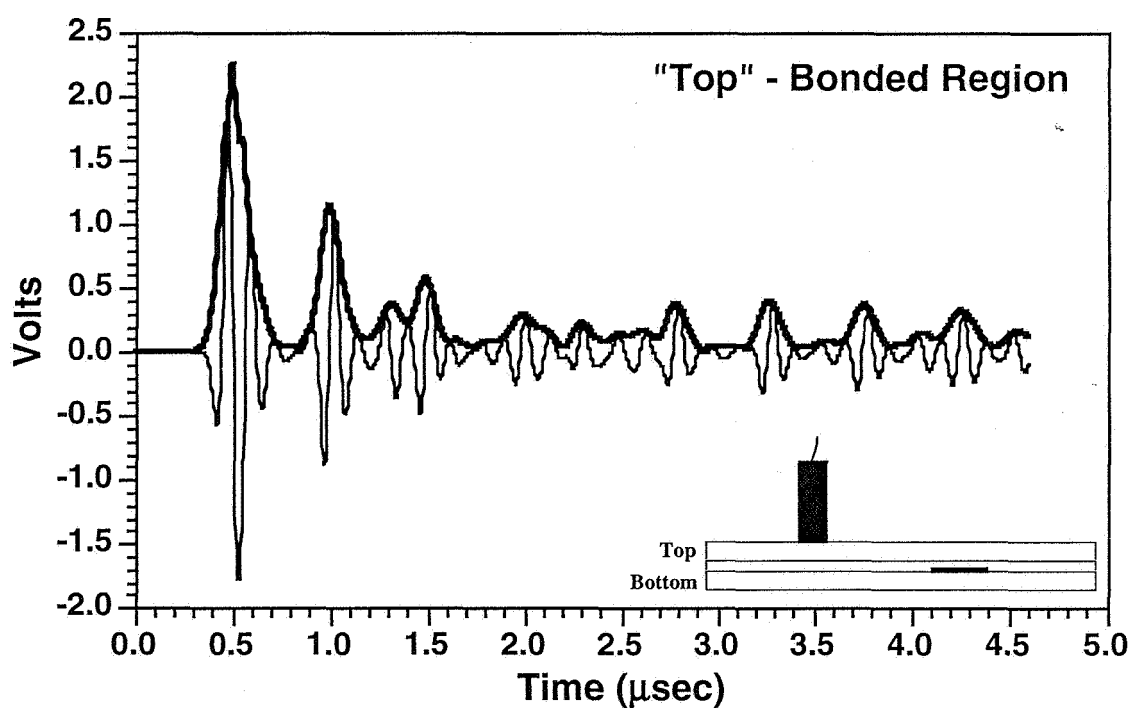


b)

**Figure 19:** The rf and analytic signal of the rf for sample E. a) Insonification of an aluminum only region b) Insonification over the epoxy strip region

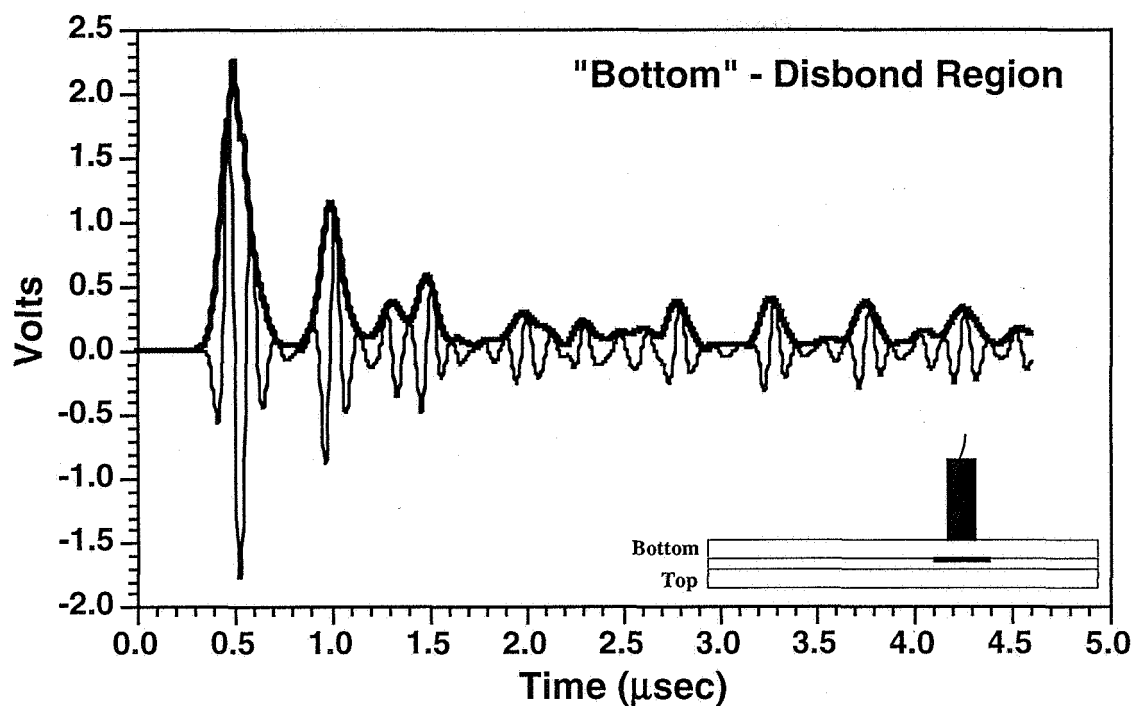


a)

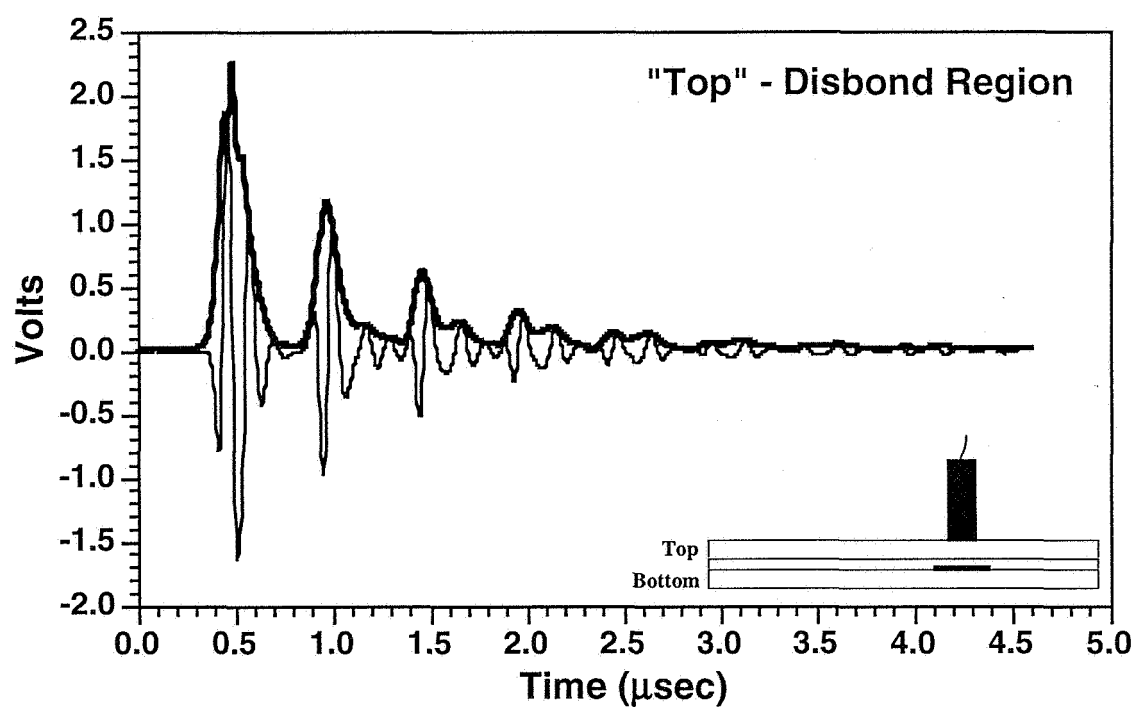


b)

**Figure 20:** The rf and analytic signal of the rf for sample F over the well-bonded area.  
 a) Insonification from the "bottom" side, the side where the paper-tape was adhered b) Insonification from the "top" side



a)



b)

**Figure 21:** The rf and analytic signal of the rf for sample F over the "disbonded" area.  
 a) Insonification from the "bottom" side, the side where the paper-tape was adhered b) Insonification from the "top" side

## **VI. Linear Array Inspection of Typical "Flaws" Encountered in Aircraft Structures**

In this Section we present results from real-time video-taped images obtained from an unmodified commercial linear-array medical scanner of specimens constructed to simulate typical types of flaws encountered in the inspection of aircraft structures. We describe the method of linear-array imaging. This section briefly reviews how the images were obtained and describes the specific specimens investigated followed by a discussion of the observations. Results of the linear array imaging were presented to NASA Langley (10/31/95 Progress Report) on an accompanying videotape.

### ***Method of Linear-Array Imaging***

An unmodified, commercially available Hewlett-Packard Sonos 2500 medical linear array imaging system was employed. The Sonos 2500 was operated in a mode that utilized a linear array of ultrasonic transducer elements as the interrogating probe. The B-scan (cross-sectional) image of the object under interrogation was formed by sequentially transmitting and receiving with groups of transducer elements across the array. Each transmission of an ultrasonic pulse and the subsequent reception of the returned signals by a specific group of transducers represents one ultrasonic A-line in a direction normal to the array. The B-scan image is produced from a series of A-lines across the aperture of the array. A depth-dependent gain (time-gain compensation or TGC) was applied to the received ultrasonic signals to reduce the effects due to the inherent attenuation of the specimen on the displayed B-scan image.

The ultrasonic signals obtained with the linear array are logarithmically compressed and displayed as a gray scale image on a dB scale. In general, each B-scan image obtained with a linear array is a cross-sectional representation of the amplitude of the reflected (scattered) ultrasonic signals, in the plane of the array, throughout the depth of the specimen under interrogation.

Because the Sonos 2500 system is intended to be used to image specific organs, vessels, and tissues in a clinical setting, it was not possible to change the depth setting of the images to more closely correspond to the thickness dimensions of the specimens. Therefore, the images obtained with the Sonos 2500 system typically represent the echo-decay patterns of many round-trip echoes. Interpretation of the images obtained from relatively thin or layered solids were expected to be somewhat complex because of the presence of strong reverberations and possible mode conversions. Because the linear array imaging system currently available is a 7.5 MHz imaging system, the test specimens were scaled such that the dimensions were more appropriate for 7.5 MHz interrogation. This does not compromise the results of the investigation



or the applicability of the linear array imaging technique to actual aircraft structures but permits us to investigate the usefulness of linear array imaging on proportionately sized specimens.

### *Specimens Investigated*

A Hewlett-Packard Sonos 2500, configured in the 7.5 MHz linear array imaging mode, was employed to interrogate a series of specimens with intentional flaws. One genre of specimen contained simulated "cracks" under fasteners. Flat-bottom holes were drilled under the fasteners (3/8" 10-32 machine screws) to represent cracks in a plane parallel to the face of the linear array probe. These specimens were interrogated in a water bath with the linear array insonifying the top surface of the specimen as illustrated in Figure 22. Duplicate flat-bottom holes were drilled midway between the fasteners to aid in the initial determination of the type of echo the investigator should look for. The dimensions of the fasteners and the simulated cracks for this type of specimen are also displayed in the figure.

Specimens designed to mimic a typical "I"-shaped stiffener support structure component (that might be found as part of the underlying airframe substructure) were investigated next. In airframe applications the flange of a stiffener is typically attached to the skin of the structure it is supporting, thus ultrasonic inspections are limited to accessing the "I"-beam through one of its flanges. To simulate the cracks in this type of support structure, flat-bottom holes were drilled in the flange and web regions as well as the region where the web connects to the flange, (referred to as the radius region). Due to the availability of material aluminum "T" 's were substituted for the "I"-shaped stiffeners. Figure 23 displays the aluminum sample dimensions and Figures 24, 25 and 26 depict the measurement setups. Specific details describing the flaw sizes, locations and imaging observations are summarized in Tables 2,3,4.

Linear array imaging techniques were applied to the interrogation of solid aluminum angles ("L" stiffeners) with flat-bottom holes of specific diameters drilled into the radius of the inclusive and exclusive angle of the "L" as depicted in Figures 27 and 28. The radii were interrogated with the right-angle specimens immersed in a water bath and the linear array positioned from the opposite side to which the flat-bottom hole was drilled. The linear array was oriented such that the images produced were formed with the array orthogonal to the plane of the right-angle. Table 5 summarizes the flaw sizes interrogated.

### *Discussion of Observations*

In this Section we summarize the findings from our interrogation of the specimens described above. The accompanying video tape (delivered with our 10/95 Progress Report to NASA Langley) displayed the linear array observations in detail.

Table 1 summarizes the observations for the linear array interrogations of the specimen containing flaws under the head of fasteners. The echoes from the flat-bottom holes under a fastener appear as short horizontal lines located between the initial front wall reflection and the first back wall reflection. All of the flaws (1/8", 1/16", and 1/32" flat-bottom holes) were discernible but the echoes decreased in brightness the smaller the hole diameter.

The observations for the linear array interrogations of flaws in the flange of "T"-shaped stiffener support structures are summarized in Table 2. The linear array was mounted to a gelatin standoff and positioned across the web of the stiffener as shown in Figure 24. The B-scan image displayed parallel horizontal lines on the left and right side of the image and a darkened region in the center of the image. The horizontal lines (echoes) represent the reverberations from the back wall of the flanges and the darkened center region the web area of the specimen. All the flat-bottom hole echoes appear as a reverberation pattern of short horizontal lines. The first echo of the pattern appears approximately midway between the front wall echo and first back wall echo from the flanges. The flaws for all the diameter flat-bottom holes were observed.

Table 3 summarizes the observations for the linear array interrogations of flaws in the web of "T"-shaped stiffener support structures. The linear array was mounted to a gelatin standoff and positioned across the web of the stiffener as illustrated in Figure 25. The B-scan image displayed parallel horizontal lines on the left and right side of the image and a darkened region in the center of the image. Again the horizontal lines (echoes) represent the reverberations from the back wall of the flanges and the darkened center region the web area of the specimen. All the flat-bottom hole echoes appear as a reverberation pattern of short horizontal lines in the darkened center region (the web region). Detection of all the flaws was achieved except for the deepest 1/4", 1/8", and the 1/32" flaws.

The observations for the flaws in the radius of "T"-shaped stiffener support structures are summarized in Table 4. The linear array was mounted to a gelatin standoff and positioned aligned along the web of the stiffener and tilted approximately 5° with respect to the normal of the flange, as depicted in Figure 26. The echo decay pattern from the flaw appears as a series of short horizontal lines interspersed with the series of horizontal lines (echoes from where the

flange connects with the web). Echoes from the flaws were most easily seen when the ultrasound impinged on the flaw perpendicular to an aluminum/flaw interface. Therefore, the slight tilting of the linear array helped to brighten the flaws echo. Detection of all the flaws was achieved except for the 1/8", 65° flaw.

Table 5 summarizes the observations for the linear array interrogations of flaws in the radius of "L"-shaped stiffener support structures. The specimens were interrogated in a water bath as illustrated in Figures 27 and 28.

The typical B-scan image for flaws drilled into the inclusive angle of the radius and insonified from the exclusive angle side displayed a wide band of white (corresponding to the initial water/specimen interface) followed by horizontal lines. The flaw appeared as a short horizontal line lying between the wide band and the horizontal line. Detection of the 1/4", 1/8", and the 1/16" flaws was achieved, but not for the 1/32" flaw.

The typical B-scan image for flaws drilled into the exclusive angle of the radius and insonified from the inclusive angle side displayed a series of parallel horizontal lines with the flaw represented by two echo decay patterns side-by-side. Each echo decay pattern consisted of short horizontal lines. The two echo decay patterns were horizontally separated by a short dark space. Detection was achieved for the 1/4", 1/8", and the 1/16" flaws, but not for the 1/32" flaw.

### *Conclusion*

These results suggest that information regarding the characteristics, location, and interface properties of specific types of flaws in materials and structures may be obtained from the images acquired with a linear array. Furthermore, linear array imaging may offer the advantage of being able to compare "good" regions with "flawed" regions simultaneously, and in real time. Real-time imaging permits the inspector to obtain image information from various views and provides the opportunity for observing the effects of introducing specific interventions. Observation of an image in real-time can offer the operator the ability to "interact" with the inspection process, thus providing new capabilities, and perhaps, new approaches to nondestructive inspections. This enhancement may aid in the probability of detection and real-time characterization of certain types of flaws.

## Flat-Bottom Hole Under Head of Fastener

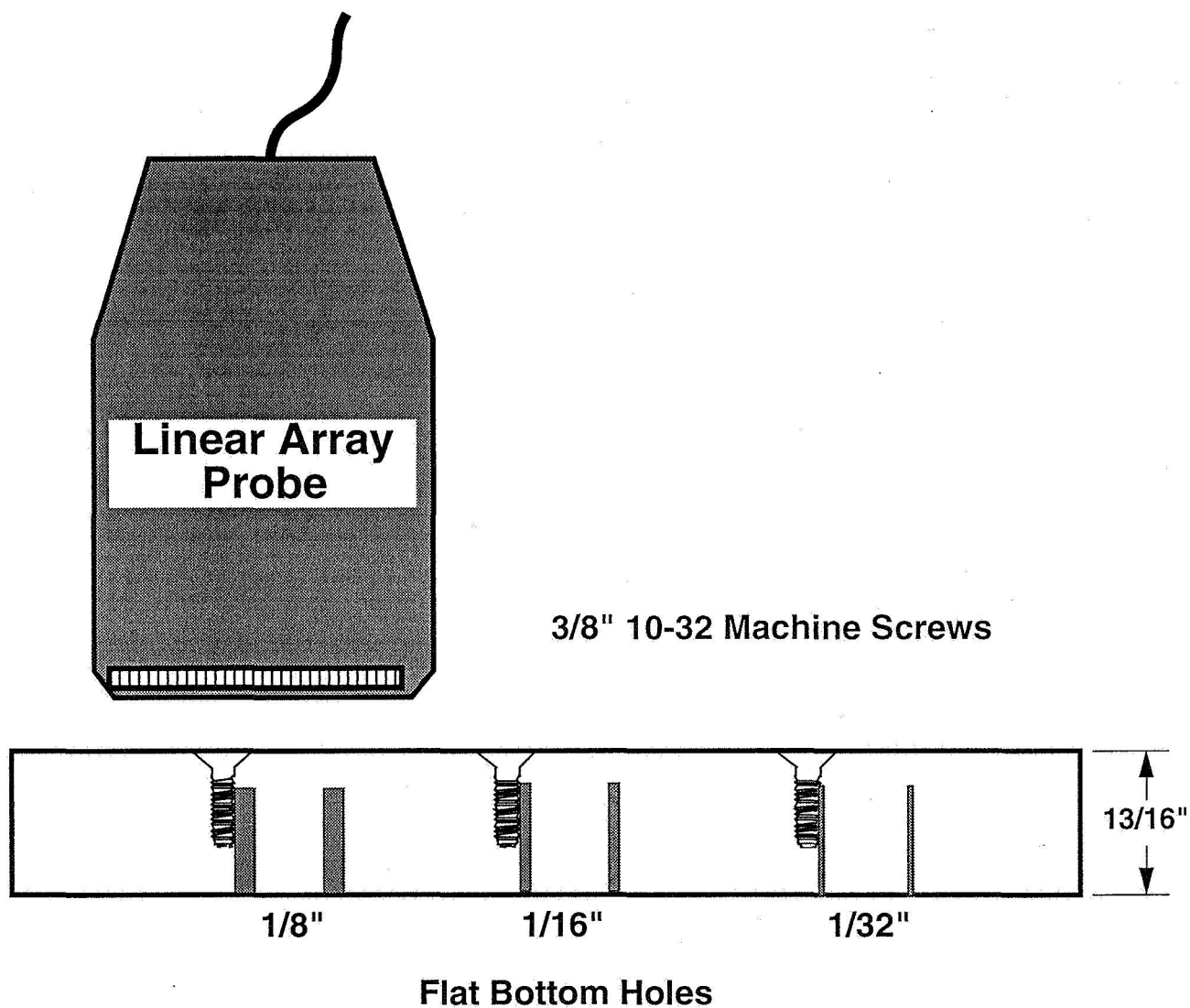


**Figure 22:** Illustration of the measurement setup for the interrogation of "flaws" located under the head of fasteners

## Aluminum "T" Dimensions

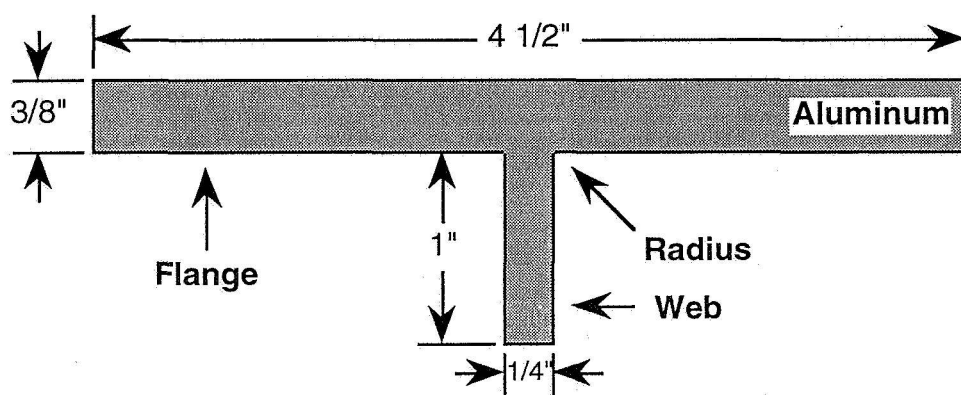


**Figure 23:** Sample dimensions for the interrogation of "flaws" in the flange, web, and radius of "I"-shaped stiffener support structures. "T"-shaped aluminum samples were substituted for the "I"-shaped stiffener.

## Flat-Bottom Hole in Flange

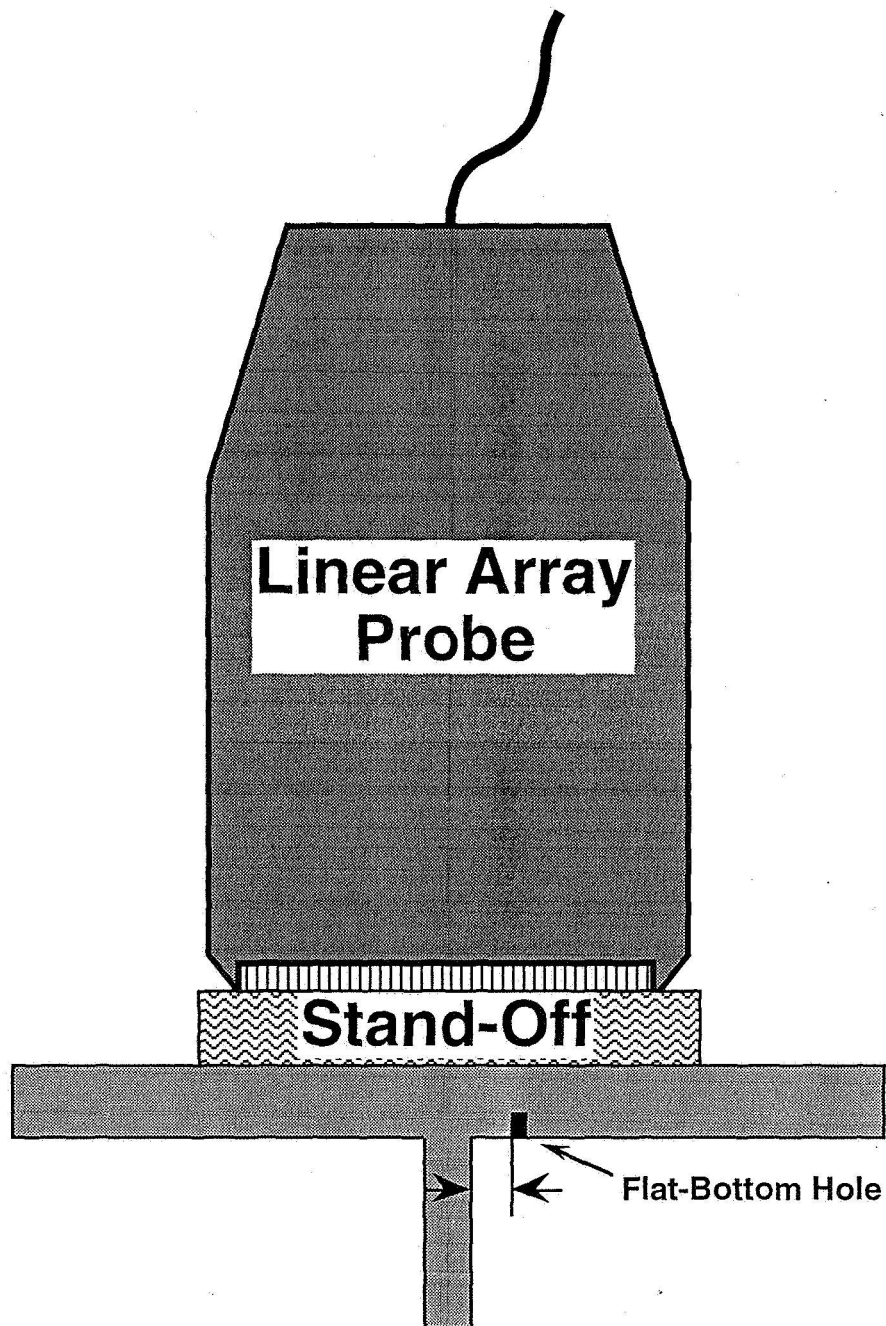


**Figure 24:** Illustration of the measurement setup for the interrogation of "flaws" in the flange of a stiffener support structure

## Flat-Bottom Hole in Web

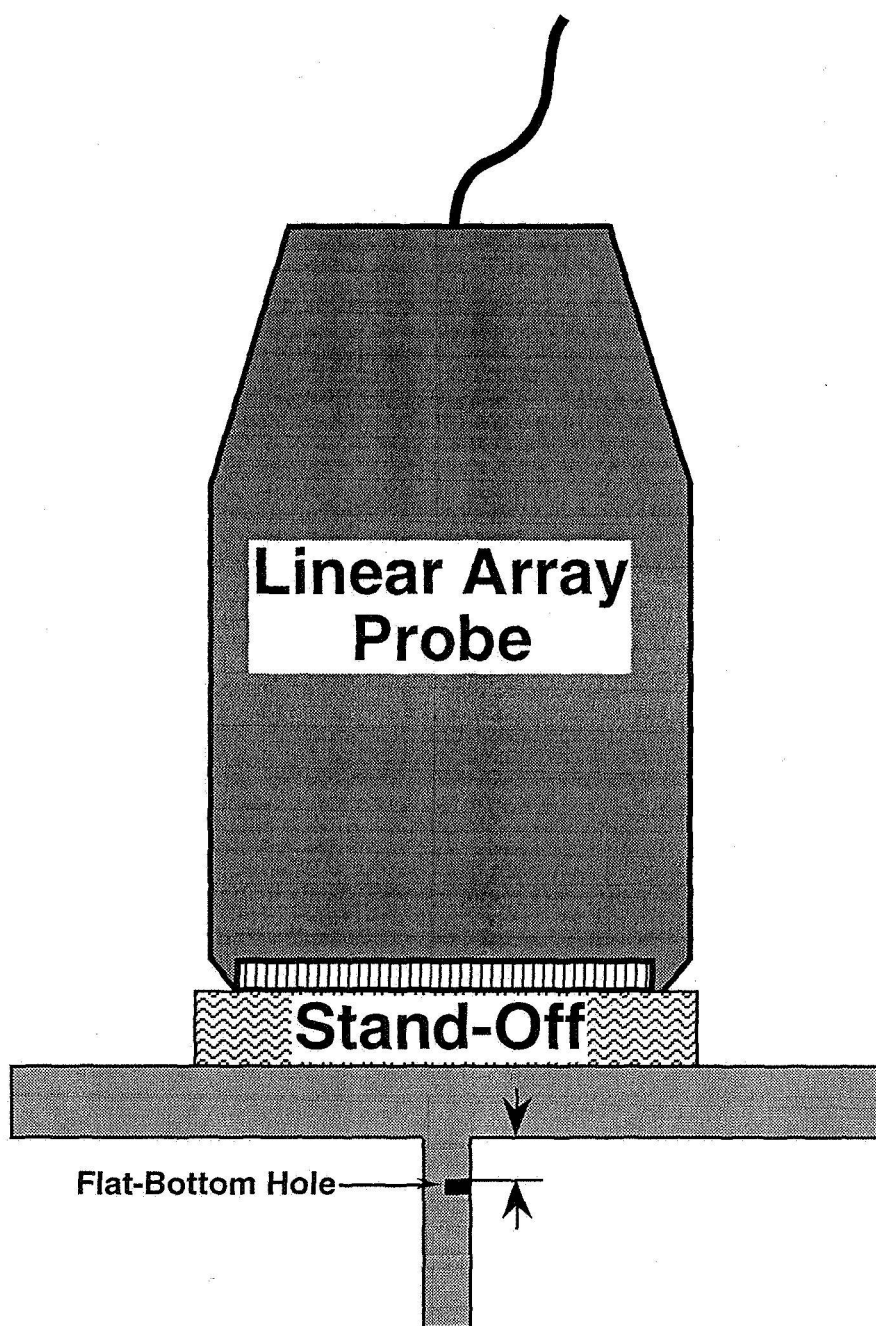


**Figure 25:** Illustration of the measurement setup for the interrogation of "flaws" in the web of a stiffener support structure

## Flat-Bottom Hole in Radius

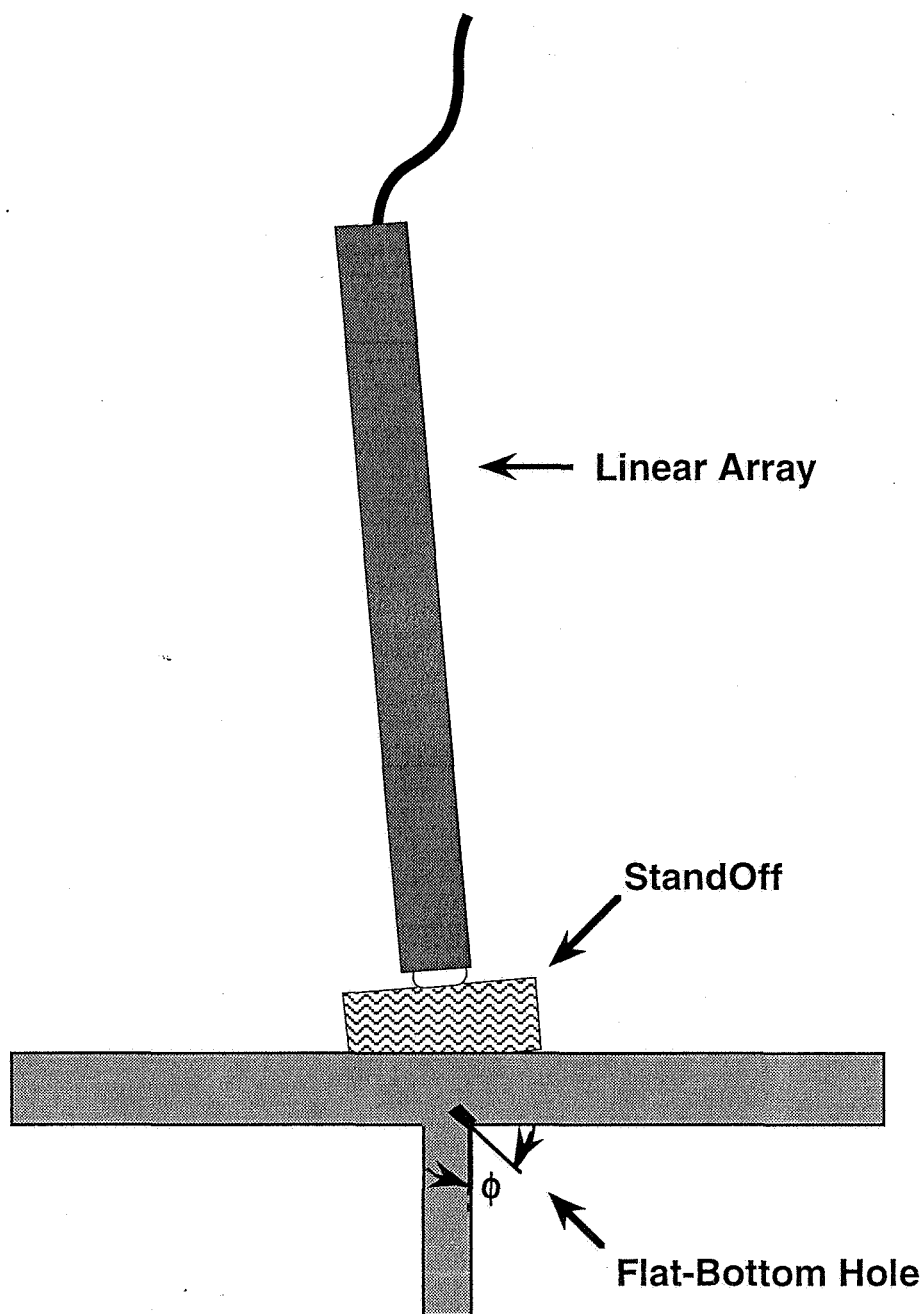


**Figure 26:** Illustration of the measurement setup for the interrogation of "flaws" in the radius of a stiffener support structure



## Flat-Bottom Hole in Inclusive Angle of "L"-Shape Stiffener

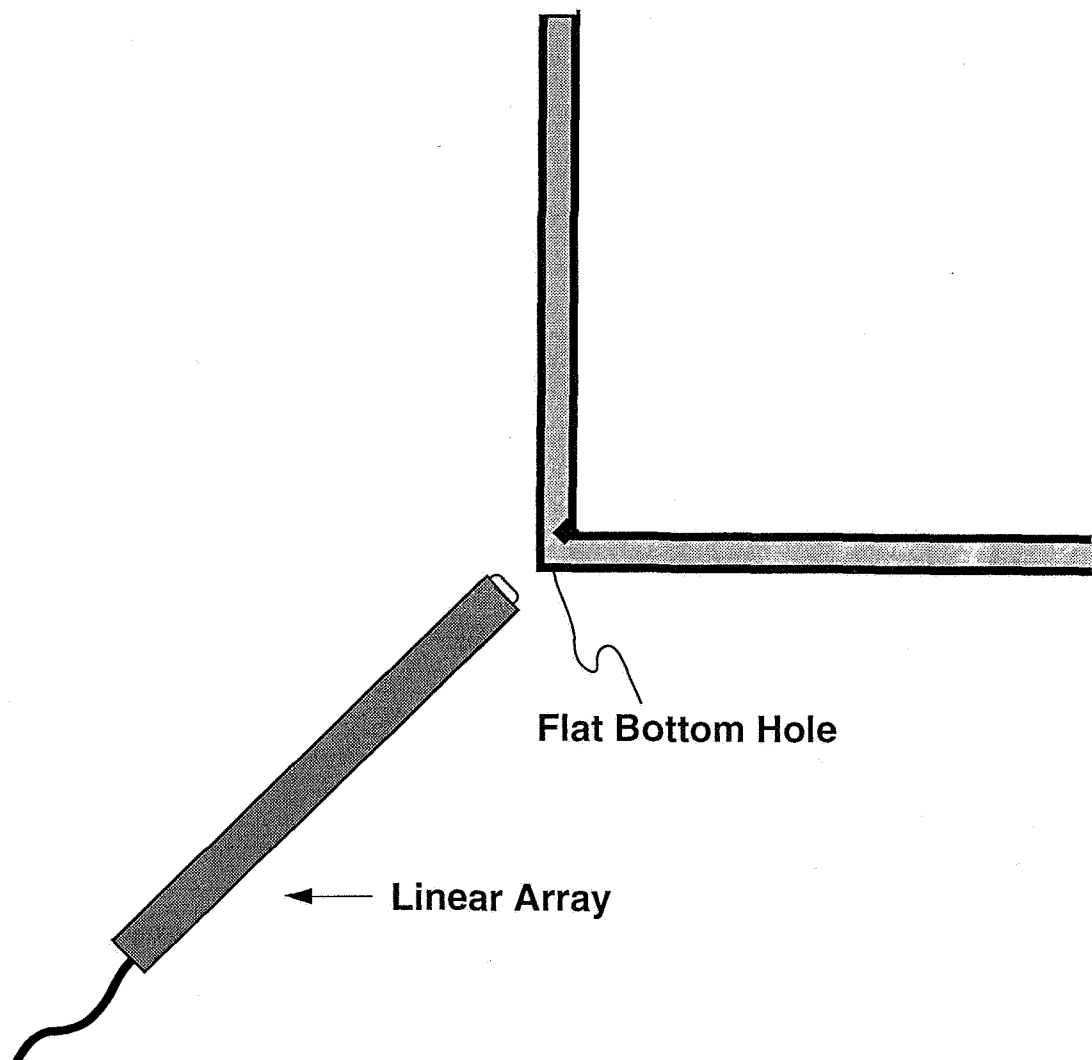


**Figure 27:** Illustration of the measurement setup for the interrogation of "flaws" in the inclusive angle of an "L"-shaped stiffener

## Flat-Bottom Hole in Exclusive Angle of "L"-Shape Stiffener

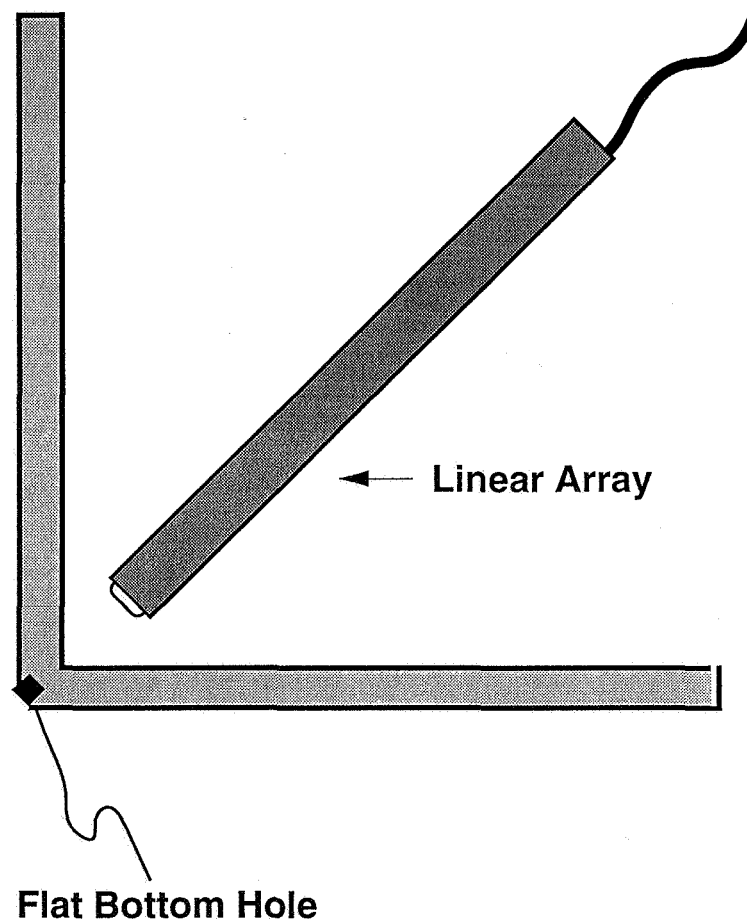


**Figure 28:** Illustration of the measurement setup for the interrogation of "flaws" in the exclusive angle of an "L"-shaped stiffener

Flat-Bottom Hole Under Head of Fasteners	
(3/8" 10-32 machine screws were used for the fasteners)	
Flat-Bottom Hole Diameter	Was the Flaw Seen?
1/8"	yes
1/16"	yes
1/32"	no

**Table 1:** Summary of the observations for the interrogation of "flaws" under the head of a fastener with the linear array imaging system

Flat-Bottom Hole in Flange of "T"		
Flat-Bottom Hole Diameter	Flat-Bottom Hole Location in the Flange (distance from outer diameter of flat-bottom hole to the side surface of the web)	Was the Flaw Seen?
1/4"	0 mm	yes
1/4"	6 mm	yes
1/4"	12 mm	yes
1/4"	15 mm	yes
1/4"	18 mm	yes
1/8"	0 mm	yes
1/8"	4 mm	yes
1/8"	10 mm	yes
1/8"	13 mm	yes
1/8"	16 mm	yes
1/16"	0 mm	yes
1/16"	4 mm	yes
1/16"	7 mm	yes
1/16"	10 mm	yes
1/16"	13 mm	yes
1/32"	0 mm	yes
1/32"	3 mm	yes
1/32"	6 mm	yes
1/32"	9 mm	yes
1/32"	12 mm	yes

**Table 2:** Summary of the observations for the interrogation of "flaws" in the flange of a "T"-shaped stiffener with the linear array imaging system

Flat-Bottom Hole in Web of "T"		
Flat-Bottom Hole Diameter	Flat-Bottom Hole Location in the Web (distance from outer diameter of flat-bottom hole to the bottom surface of the flange)	Was the Flaw Seen?
1/4"	0 mm	yes
1/4"	6 mm	yes
1/4"	13 mm	yes
1/4"	18 mm	no
1/8"	0 mm	yes
1/8"	7 mm	yes
1/8"	13 mm	yes
1/8"	20 mm	no
1/16"	0 mm	yes
1/16"	7 mm	yes
1/16"	14 mm	yes
1/16"	20 mm	yes
1/32"	0 mm	yes
1/32"	6 mm	yes
1/32"	12 mm	yes
1/32"	18.5 mm	no

**Table 3:** Summary of the observations for the interrogation of "flaws" in the web of a "T"-shaped stiffener with the linear array imaging system

Flat-Bottom Hole in Radius of "T"		
Flat-Bottom Hole Diameter	Flat-Bottom Hole Angle in the Web (angle measured with respect to the web)	Was the Flaw Seen?
1/4"	0 degrees	yes
1/4"	25 degrees	yes
1/4"	45 degrees	yes
1/4"	65 degrees	yes
1/4"	90 degrees	yes
1/8"	0 degrees	yes
1/8"	25 degrees	yes
1/8"	45 degrees	yes
1/8"	65 degrees	no
1/8"	90 degrees	yes
1/16"	0 degrees	yes
1/16"	25 degrees	yes
1/16"	45 degrees	yes
1/16"	65 degrees	yes
1/16"	90 degrees	yes
1/32"	0 degrees	yes
1/32"	25 degrees	yes
1/32"	45 degrees	yes
1/32"	65 degrees	yes
1/32"	90 degrees	yes

**Table 4:** Summary of the observations for the interrogation of "flaws" in the radius of a "T"-shaped stiffener with the linear array imaging system

Flat-Bottom Hole in the Radius of an "L"-Stiffener		
Flat-Bottom Hole Diameter	Flat-Bottom Hole Location	Was the Flaw Seen?
1/4"	Drilled in the inclusive angle	yes
1/8"	Drilled in the inclusive angle	yes
1/16"	Drilled in the inclusive angle	yes
1/32"	Drilled in the inclusive angle	no
1/4"	Drilled in the exclusive angle	yes
1/8"	Drilled in the exclusive angle	yes
1/16"	Drilled in the exclusive angle	yes
1/32"	Drilled in the exclusive angle	no

**Table 5:** Summary of the observations for the interrogation of "flaws" in the radius of a "L"-shaped stiffener with the linear array imaging system

## References:

1. Steven N. Bobo, "The Aging Aircraft Fleet: A Challenge for Nondestructive Inspection", *Review of Progress in Quantitative Nondestructive Evaluation* (Brunswick, ME, 1990), D.O. Thompson and D.E. Chimentis, Eds. , Vol. 9, pp. 2097-2109, Plenum Publishing Corporation,
2. Chris Seher and Alfred L. Broz, "National Research Program for Nondestructive Inspection of Aging Aircraft", *Materials Evaluation*, Vol. 49, pp. 1547-1550, (1991).
3. Frank A. Iddings, "Large-Area Aircraft Scanner", *Review of Progress in Quantitative Nondestructive Evaluation* (Brunswick, ME, 1992), D.O. Thompson and D.E. Chimentis, Eds. , Vol. 11, pp. 2233-2240, Plenum Publishing Corporation,
4. T. C. Patton and D. K. Hsu, "Ultrasonic NDE of Adhesive and Sealant Bonded Aluminum Lap Joints", *Review of Progress in Quantitative Nondestructive Evaluation* (Brunswick, ME, 1992), D.O. Thompson and D.E. Chimentis, Eds. , Vol. 11, pp. 1299-1306, Plenum Publishing Corporation,
5. D. K. Hsu, M. S. Hughes, and T.C. Patton, "Ultrasonic Scans Using Low Frequency Unresolved Echoes", *Review of Progress in Quantitative Nondestructive Evaluation* (Brunswick, ME, 1993), D.O. Thompson and D.E. Chimentis, Eds. , Vol. 12, pp. 1595-1602, Plenum Publishing Corporation,
6. M. N. Abedin, D. R. Prabhu, W .P. Winfree, and P. H. Johnston, "A Comparative Study of Experimental and Simulated Ultrasonic Pulse-Echo Signals from Multilayered Structures", *Review of Progress in Quantitative Nondestructive Evaluation* (Brunswick, ME, 1992), D.O. Thompson and D.E. Chimentis, Eds. , Vol. 11, pp. 1959-1966, Plenum Publishing Corporation,
7. M. N. Abedin, P. H. Johnston, and D. R. Prabhu, "Disbond Detection Using Peak Amplitude of Pulse-Echo Signals for Various Thicknesses and Transducer Frequencies", *Review of Progress in Quantitative Nondestructive Evaluation* 1993), D.O. Thompson and D.E. Chimentis, Eds. , Vol. 12, pp. 1539-1546, Plenum Publishing Corporation,
8. Robert Dunki-Jacobs and Lewis J Thomas, "Real-Time B-Scan Ultrasonic Imaging Using a Digital Phased Array System for NDE", *Review of Progress in Quantitative Nondestructive Evaluation* (Brunswick, ME, 1992), D.O. Thompson and D.E. Chimentis, Eds. , Vol. 11, pp. 805-812, Plenum Publishing Corporation,
9. Hermann Wustenberg, Bernard Rotter, Hans Peter Klanke, and Dieter Harbecke, "Ultrasonic Phased Arrays for Nondestructive Inspection of Forgings", *Materials Evaluation*, Vol. 51, pp. 669-812, (1993).



10. G. J. Posakony, "Acoustic Imaging - A Review of Current Techniques for Utilizing Ultrasonic Linear Arrays for Producing Images of Flaws in Solids", *Elastic Waves and Non-Destructive Testing of Materials (ASME-AMD)* 1978), 29, pp. 53 -69,
11. Mark R. Holland, Patrick H. Johnston, Scott M. Handley, and James G. Miller, "Detection of Disbonded Regions in Bonded Aluminum Plates Using An Ultrasonic 7.5 MHZ Linear Array Medical Imaging System", *Review of Progress in QNDE* (Snowmass, 1994), D.O. Thompson and D.E. Chimentis, Eds. , Vol. 14B, pp. 1513-1520, Plenum Press, 1995.
12. "Tissue-Simulating Gel for Medical Research", NASA Langley Research Center, Report Number: LAR-14036, (1993).